Numerical analysis of a hybrid cooling tower and its plume

by

Aditya Kodkani

A thesis submitted in partial fulfillment of the requirements for the degree of

Master of Science

Department of Mechanical Engineering
UNIVERSITY OF ALBERTA

Abstract

The most practical and economical method of dissipating waste heat from power stations, and related heavy industry is via wet cooling towers. These towers dissipate the waste heat present in a stream of hot process water primarily by evaporating some small fraction of this water, which, in turn, leads to evaporative cooling. As a byproduct of this evaporation, wet cooling towers must emit to the atmosphere air that is hot and moist. Under select climatic conditions (e.g. cold ambient air with an elevated relative humidity), a visible plume may form. Such a plume is considered a public nuisance and may lead to an unwanted accumulation of moisture or, worse yet, ice on surrounding infrastructure e.g. roadways, runways and industrial facilities. To avoid such undesirable outcomes and to conserve water, a combination of wet and dry cooling may be employed in a hybrid cooling tower. To design a hybrid cooling tower for effective visible plume abatement, one requires not only knowledge of the turbulent mixing characteristics of the atmospheric plume but, in tandem, a model that describes heat and mass transfer processes within the cooling tower itself.

This thesis presents a mathematical model to study the heat and mass transfer inside a hybrid cooling tower and a model to predict the behaviour of the atmospheric plume. The wet-portion model expands upon one presented in the earlier study of Klimanek and Bialecki (Int. Commun Heat Mass 36:547-553, 2009) by assigning zone-specific Merkel numbers to each of the rain, fill, and spray zones. Accordingly, we can determine, zone-by-zone, rates of heat rejection and water evaporation. By extension, we can estimate the mass flow rate of water and the humidity ratio and related thermodynamic properties of the outlet air and water streams. Our augmented model is validated against the well-established Poppe and Merkel methods as well as select field data from a multi-cell cooling tower located in Colorado, USA.

A turbulent plume model based on the conservation of mass, momentum, heat, and moisture is adapted from the work of Wu and Koh (1978) [1] is coupled with the tower model described above. As a result, we are able to predict the behavior of plumes emanating from multiple cooling tower cells. By extension, predictions of the likelihood of fog formation and, where applicable, of the visible plume height may be made. Special reference is made to ambient states characterized as hot-dry, hot-humid, cool-dry, and cool-humid to study cooling tower performance under a variety of climatic conditions.

Preface

I, Aditya Kodkani, declare that this thesis titled, 'Numerical analysis of hybrid cooling towers and its plume' and the work presented in it are my own. Furthermore, permission is hereby granted to the University of Alberta Libraries to reproduce single copies of this thesis and to lend or sell such copies for private, scholarly or scientific research purposes only. Where the thesis is converted to, or otherwise made available in digital form, the University of Alberta will advise potential users of the thesis of these terms.

The author reserves all other publication and other rights in association with the copyright in the thesis and, except as herein before provided, neither the thesis nor any substantial portion thereof may be printed or otherwise reproduced in any material form whatsoever without the author's prior written permission.

Acknowledgements

This thesis becomes a reality with the kind support and help of many individuals; I would like to extend my sincere thanks to all.

I would like to express my sincere to my advisers Prof. Morris R Flynn and Prof. Marc Secanell for their support throughout the development of this thesis. Finally, I would like to acknowledge the support provided by Natural Sciences and Engineering Research of Canada (NSERC) through a Collaborative Research and Development Grant generously co-sponsored by International Cooling Tower Inc.

Contents

List of Tables

List of Figures

Abbreviations

CFD	Computational Fluid Dynamics
VFD	Variable Frequency Drive
PPWD	Parallel Path Wet Dry
NTU	Number of Transfer Units
LMTD	Log Mean Temperature Difference

Nomenclature

A	Area, m^2
a_f	Interface area, m^2
c_p	Specific heat at constant pressure, J/kgK
d	diameter, m
h	Enthalpy, J/kg
k	Thermal conductivity, W/mK
m	Mass flow rate, kg/s
P	Pitch, m
Q	Heat transfer rate, W
r_0	Latent heat of vaporization measured at $T_w = 0°C, J/kg$
T	Temperature, K
t	Thickness, m
H	Height, m
M	Momentum flux, m^4/s^2
P	Pressure, $kg/m\,s^2$
Q	Volume flux, m^3/s

Dimensionless group

Le_f Lewis factor

Nu Nusselt number

Pr Prandtl number

Re Reynolds number

Greek Symbols

α Average heat transfer coefficient, $\mathrm{W/m^2K}$

β Average mass transfer coefficient, $\mathrm{Kg/m^2s}$

γ Entrainment coefficient

μ Dynamic viscosity, $\mathrm{kg/(m\,s)}$

ω Humidity ratio, kg/kg

ρ Density, $\mathrm{kg/m^3}$

Subscripts

a Air

evp Evaporation

f fin

fi Fill zone

p Plume

rz Rain zone

s Saturation

sp Spray zone

v Vapor

w Water

Chapter 1

Introduction

1.1 Background

A cooling tower is a heat exchanger device used to reject the low-grade heat that is generated as a byproduct of doing mechanical work. For the efficient functioning of power stations and other process industries like oil refineries or petrochemical/metallurgical plants, the low-grade heat has to be rejected to the atmosphere or the hydrosphere. Cooling towers are used to dissipate heat to the atmosphere whereas, once-through cooling systems are used to transfer heat to a nearby water source, such as a lake or river [2, 3].

With a once-through cooling system, the water from a nearby source is used for dissipating the heat via heat exchangers and the hot water, having a temperature of approximately 60°C or higher, is dumped back into its source [4]. This type of cooling is environmentally unacceptable as the hot water creates the right environmental conditions for an algae bloom. Algae blooms can negatively affect marine ecology by depleting the concentration of dissolved oxygen or by preventing sunlight from reaching lake or riverbeds [5]. With stringent environmental restrictions and locales where ample water sources did not exist, wet cooling towers came to be regarded as a more palatable alternative to once-through cooling systems.

In a wet cooling tower, heat transfer occurs as a result of both sensible and, more especially, latent effects; the process water is in direct contact with the ambient air leading to evaporative cooling. Owing to this evaporation, and the consequent loss of water to the atmosphere, approximately 1 to 2% of the total mass flow rate of water

has to be replenished to make up for the water evaporated [4]. Another problem with wet cooling towers that has gained attention in recent years is visible plume formation. Visible plumes from cooling towers are generally considered a public nuisance as they can lead to a health [6] or visibility hazards [2, 7]. In order to avoid visible plumes and to conserve water, engineers developed methods for dry cooling, whether used in conjunction with, or to the exclusion of, wet cooling.

In a dry cooling tower, heat transfer occurs through sensible effects; the hot process water passes through a finned air heat exchanger where the process water and the ambient air are not in direct contact (non-evaporative cooling). Dry cooling towers have virtually no harmful impact on the environment, as they release only warm and clean air. However, they require high capital and operating investments and have a larger area footprint. It is estimated that a dry cooling tower costs 1.6 to 1.7 times as much as its wet tower counterpart for similar ambient conditions and design points [8]. Furthermore, they are inefficient when the ambient temperature is warm, which might lead to performance penalties. To overcome the shortcomings of dry towers a combination of wet and dry (hybrid) cooling towers is sometimes applied as shown in Figure 1.1. Hybrid cooling and its promise of partial or full visible plume abatement is especially attractive when fog formation is deemed undesirable and/or is restricted by regulatory agencies.

Hybrid cooling towers provide advantages over conventional wet and dry cooling towers in terms of water conservation, visible plume abatement, size flexibility, sensitivity to ambient conditions, and thermal discharge. Given this advantage, there is a need for a mathematical model that can predict with good precision those combinations of operating and environmental conditions that are likely to result in fog formation. To this end, one requires not only knowledge of the turbulent mixing characteristics of the atmospheric plume but, in tandem, a model that describes heat and mass transfer processes within the tower itself. This study aims to develop a mathematical model that can determine the visible plume height, and also the heat and mass transfer process happening in a hybrid cooling tower for given ambient conditions.

1.2 Cooling tower classification

Cooling towers can be further classified based on the methods used to generate airflow and the air-to-water flow arrangement. In terms of airflow generation, towers can be

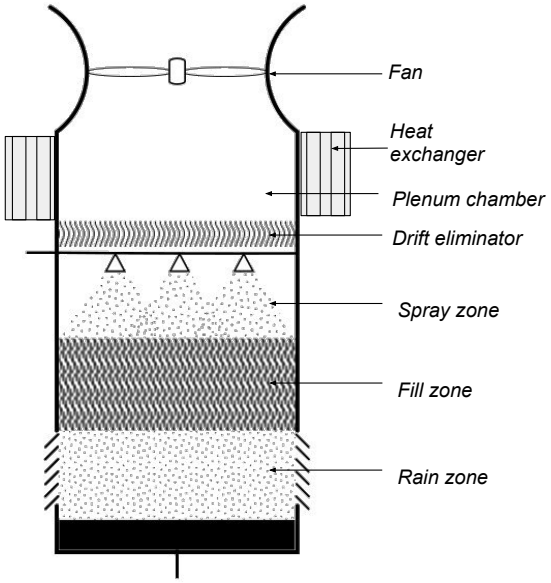

FIGURE 1.1: A schematic of a hybrid cooling tower.

classified as mechanical-type vs. natural draft-type. In a natural draft cooling tower, airflow is driven by the density difference between the air inside of the tower vs. that in the external ambient. These types of towers are generally used for dissipating large heat loads. On the other hand, mechanical draft cooling towers are relatively small structures compared to natural draft towers. Air can be either blown into the tower with a fan at the bottom (forced draft) or drawn upwards through the tower with a fan at the top (induced draft). A further classification is based on the airflow arrangement, i.e. counterflow vs. crossflow. In crossflow, the air flows perpendicular to the water flow whereas in counterflow the air flows anti-parallel to water. A detailed comparison between counterflow and crossflow cooling towers is provided in Table 1.1. Given this wide design space, we here choose to focus on induced draft wet cooling towers in counterflow as they are widely used in industry [9].

1.3 Working principle of a hybrid cooling tower

hot process water and the ambient air enter the dry section which results in a sensible heating of ambient air from the process water. The sensible heating is represented as a horizontal line in the psychrometric chart of Figure 1.2. The heat is added to the ambient air that is at a constant moisture content (i.e. along line joining the two points 1 and 3 in Figure 1.2), the partially cooled water from the dry section enters a wet

TABLE 1.1: Comparison between counterflow and crossflow cooling towers [4, 6]

	Counterflow	Crossflow
Air recirculating	Less risk of recirculation	More risk of recirculation due to tall inlet height
Maintenance	Less prone to dirt and algae growth	More prone to algae growth and not recommended for use in a dusty environment
Initial cost	High installation cost	Low installation cost
Area	Small footprint	Large footprint
Future expansion	Fill height can be easily increased	No capacity to increase fill height
Fan power consumption	Low power consumption due to lower rate of airflow	High power consumption due to higher rate of airflow

section for further cooling.

The wet section of a hybrid cooling tower has three critical zones. Following the path of the water, these are the spray zone, the fill zone, and the rain zone. The former represents the point of entry to the tower of the hot water, which is discharged through a series of spray nozzles. The primary function of a spray zone is to distribute the water evenly across the underlying fill (Note, however, that some cooling may occur in the spray zone, i.e. up to 15% of total cooling according to Kröger [4]). Based on the geometry of the fill chosen, the water may break into smaller droplets or may form a thin film over closely packed, vertically-aligned plates. In either case, the surface area and air-water contact time are increased, and thus the fill zone accounts for 65-80% of the total cooling [4]. From the fill, the water drips down unobstructed into a water basin through a portion of the tower known as the rain zone. The rain zone accounts for 10-20% [4] of total cooling. A drift eliminator may be placed above the spray zone to prevent small droplets of liquid water escaping from the top of a cooling tower. Addition of latent and sensible heat to the ambient air in the wet section results in the increase of air temperature and moisture, which is represented by a line joining the points 1 to 2 in Figure 1.2.

The two air streams from the wet (hot-humid air) and dry sections (hot-dry air) converge in a plenum chamber. For example, if an equal proportion of air entering the plenum chamber from the dry and wet sections, the quality of the resulting mixed air leaving the cooling tower will lie halfway between points 2 and 3, which is represented by point 4 in Figure 1.2. As the line connecting 1 to 4 falls below the saturation curve, there is no visible plume.

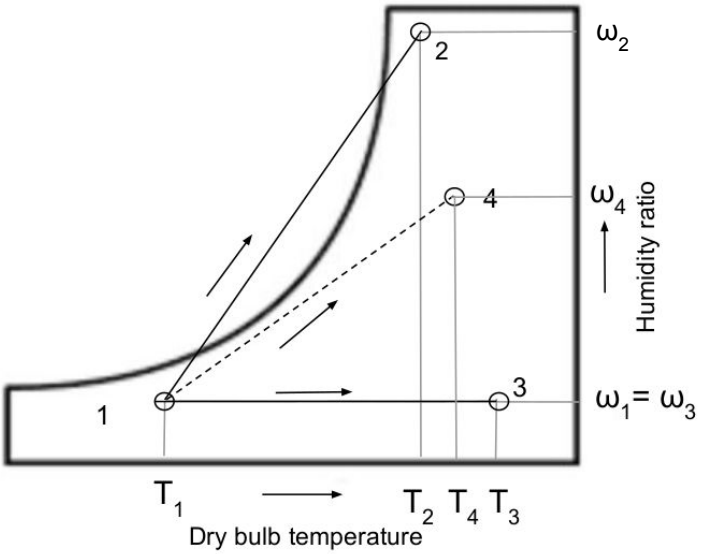

FIGURE 1.2: Psychrometric chart for representing the air quality in a hybrid cooling tower. In this Figure, point 1 represents the ambient air condition, point 2 denotes the quality of air leaving the wet section, point 3 indicates the quality of air leaving the dry section, and point 4 denotes the quality of air leaving the tower.

1.4 Visible plume

Visible plumes are generally considered undesirable, particularly when cooling towers are located in close proximity to residential neighborhoods or critical infrastructure such as highways, airports and industrial facilities where icing and/or lack of visibility pose threats to safety. Furthermore, the water droplets within the visible plume can spread bacteria like Legionella, which can potentially cause Legionnaires' disease [6]. Visible plumes are more prevalent during winter and in humid environments. When the saturated or supersaturated (hot and humid) discharge air from a cooling tower comes in contact with ambient air, the temperature of the discharged air decreases rapidly resulting in an equally rapid increase of the relative humidity. Any excess moisture in the air stream condenses to form tiny water droplets, which render the plume visible. The various stages of plume formation can be shown using a psychrometric chart as shown in Figure 1.3. Assume the quality of air leaving the cooling tower (plume source) is represented by point 1, and the cold, humid ambient air is represented by point 4. As the plume evolves it may follow a line 1-4, at point 2, water vapor begins to condense, thus rendering the plume visible. Fog persists until the plume reaches point 3 in the psychrometric chart. At this point, the plume becomes invisible. If, on the other hand, the ambient temperature increased, the plume might instead follow the

trajectory suggested by line 1-5. Here, no intersection with the saturation curve occurs and a visible plume is not, therefore, expected.

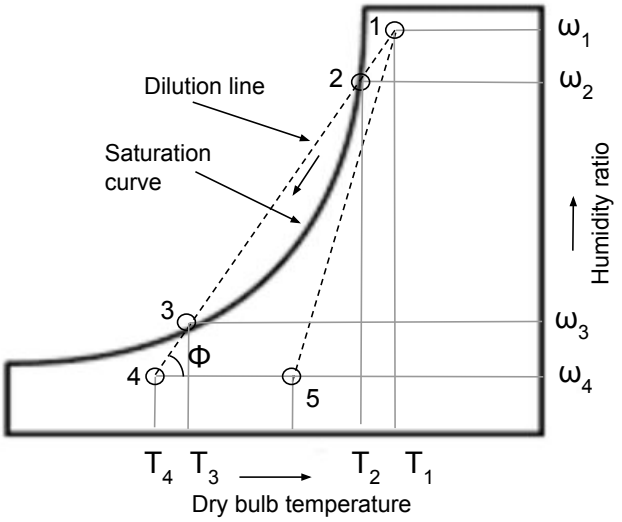

FIGURE 1.3: Psychrometric chart representing different stages of a plume. Here point 1 indicates the quality of air leaving the cooling tower, point 2 and point 3 represents the beginning and the ending of the condensation process, point 4 and point 5 denotes ambient air temperature corresponding to cold and hot conditions, finally, ϕ represents the plume abatement angle.

The common metrics used for predicting the plume severity using a psychrometric chart are the mixing line ratio and the plume abatement angle. By the former measure, the plume severity is defined as the ratio of the change in relative humidity ratio between the points of plume condensation and evaporation (points 2 and 3 in Figure 1.3) relative to the total change in relative humidity ratio (points 1 and 4 in Figure 1.3) i.e.

$$\text{Plume severity} = \frac{\omega_2 - \omega_3}{\omega_1 - \omega_4} \text{ or } \frac{T_2 - T_3}{T_1 - T_4} \tag{1.1}$$

A plume severity of 0 indicates no visible plume as the dilution line never intersects the saturation curve. By contrast, a plume severity of 1 would yield a long visible plume as the dilution line is fully within the supersaturation region. By the latter measure, the plume severity is measured by the angle between the dilution line and the horizontal as shown in Figure 1.3. Corlet et al. [10] reported that the above metrics are inconsistent and represent an incomplete picture of predicting the visible plume severity, because fogging may or may not occur for the same plume abatement angle.

1.5 Literature review

To study the performance of hybrid cooling towers Loscutoff [11] studied different combinations of wet and dry sections on the basis of the water and air flow circuits. He concluded that parallel path airflow and series water flow in the order dry-before-wet (also known as parallel path wet dry) is the best arrangement. This configuration includes parallel air inlet paths, which contribute to plume abatement and water conservation. Wanchai and Mantheerapol [12] studied the performance of a hybrid cooling tower by performing a series of experiments aimed quantifying key performance metrics. Their study showed that the performance of a hybrid cooling tower depends on the water to air (L/G) ratio in both dry and wet sections. Dehaghani and Hmadikia [13] reported that a hybrid cooling tower consumes 9.4% less make up water when compared its wet counterpart. Furthermore, they reported a 64.6% reduction in electrical (fan) power consumption when an optimum value of L/G ratio is selected.

To design a wet cooling tower, the most commonly used 0D/1D models are those described as Merkel [14], e-NTU [15], Poppe [16], and Klimanek [17]. Merkel proposed his model in 1925; it simplifies the 1D heat and mass transfer equations using a variety of assumptions, e.g. (i) The Lewis factor, Le_f, which prescribes the ratio of the heat transfer Stanton number to the mass transfer Stanton number, is considered to be unity; (ii) The air exiting the tower is saturated with water vapour and; (iii) Water loss due to evaporation is negligibly small [14, 18]. The validity of these assumptions has been considered in a variety of previous studies with different researchers surmising that the Merkel model leads to either an over- or an under-prediction of the outlet air temperature and relative humidity ratio [19–21]. Such discrepancies are not without their significance, e.g. Kloppers [22] noted that it is important to evaluate tower outlet conditions accurately in order to predict the evolution of the atmospheric plume.

To overcome the shortcomings of the Merkel model, Poppe and Rogener [16] later proposed a model that includes a more realistic description of evaporation and which relaxes the requirement of saturation, i.e. Merkel's assumption (ii) Another useful extension of Merkel is due to Klimanek and Bialecki [17] whose methodology yields the spatial distribution of key flow parameters within the tower. Importantly, however, their analysis remains "lumped" in the sense that the Merkel number defined by Klimanek and Bialecki [17] corresponds to a representative average for the cooling tower as a whole. Although this approach is computationally efficient, one cannot then comprehensively assess performance within any one of the spray, fill, or rain zones. As a consequence, it is difficult to estimate the point at which the air becomes fully saturated.

Nor is it straightforward to quantitatively predict the relative cooling contribution of these different zones.

To study the evolution of a thermal plume for given environmental conditions, Morton [23] developed a model based on the conservation of mass, momentum, energy, and moisture. The work of Morton was further extended by Csanady [24] by including an ambient wind speed to predict the visible plume height. Wigley and Slawson [25] studied the growth of moist plumes for different ambient conditions and concluded that visible plumes form close to the top of the cooling tower and that their height may be limited, particularly when the atmosphere is dry and mixing is occurs relatively rapidly. Li et al. [26] studied cooling tower plume abatement by coupling a tower model with Wu and Koh's [1] model describing the merger of adjacent plumes. They were able to identify the regime where a coaxial plume structure can offer some advantage over its uniform plume counterpart vis-à-vis plume abatement. However, Li et al.'s cooling tower model is based on an e-NTU description, which is subject to the same limiting assumptions as Merkel [26]. As such, their model predictions are expected to be less robust than had they instead used e.g. a Poppe or Klimanek cooling tower model.

1.6 Objective

Like Li et al. [26], a central goal of this work is to couple together a cooling tower model with a model describing the dispersion of the resulting atmospheric plume. In the present case, however, greater care is taken in developing and applying the cooling tower model. More precisely, we augment the model of Klimanek and Bialecki [17] so the variation of key thermodynamic variables may be predicted at different vertical locations within the cooling tower. We thereby derive accurate estimates for the conditions at the tower exit/plume source, an essential prerequisite for predicting whether or not a visible plume will form. Our model can also predict the fraction of cooling that occurs within each of the spray, fill and rain zones, a critical detail of any robust engineering design. By leveraging these predictive capabilities, we both draw comparisons between our model results vs. those stemming from related studies and also contrast cooling tower performance in a variety of climactic scenarios. Stated more succinctly, the objectives of this thesis are as follows:

- To extend the work done of Klimanek and Bialecki [17] to develop an augmented cooling tower model that predicts thermodynamic properties within a cooling tower as a continuous function of height.

- To couple the turbulent plume model developed by Wu and Koh [1] with the developed hybrid cooling tower model.

In addressing the above points, we will derive a cooling tower model capable of predicting, for example, the elevation at which air becomes saturated with water and the relative contributions to cooling of the different cooling tower zones. A model having such predictive capabilities is expected to be highly useful in the engineering design context.

1.7 Thesis Structure

This thesis is organized as follows:

- Chapter 1: Introduces the motivation for studying hybrid cooling tower and its plume and outlines the thesis objective, thesis goals, contributions, and thesis structure.
- Chapter 2: Presents a detailed derivation of the governing equations used for evaluating the thermodynamic properties of a hybrid cooling tower. The empirical equations used for evaluating key of transfer functions are also discussed.
- Chapter 3: Presents a detailed derivation of the governing equation for a turbulent plume in a uniform ambient. This chapter also discusses the criteria for plume merger in the case of multiple cooling tower cells.
- chapter 4: The developed wet cooling tower model is validated against the well-established Poppe and Merkel methods as well as selected field data. The performance of wet and hybrid cooling towers are then critically evaluated for a variety of climatic conditions.
- Chapter 5: In this chapter, the conclusion of the individual chapter are summarized and suggestions for future work are discussed.

Chapter 2

Cooling tower model

2.1 Introduction

In this chapter, the governing equations describing heat and mass transfer in a hybrid tower are derived. The first part of this chapter includes a detailed derivation of the equations relevant to the wet section. A set of four ODEs is derived, which describes the spatial distributions of key flow parameters e.g. mass flow rate of water, the relative humidity ratio and the temperatures of air and water. Thereafter, we present a discussion regarding the empirical equations necessary for determining transfer coefficients in a wet cooling tower. The second half of this chapter considers an e-NTU model, which is employed to study the dry section in a hybrid cooling tower. This chapter concludes with a discussion on the plenum chamber, wherein we evaluate parameters required for the turbulent plume model, which is discussed in the subsequent chapter.

2.2 Wet cooling

In cooling towers, process water is cooled by interacting with ambient air. As the hot water falls down the tower, it comes into contact with the ambient air whose upward flow is, for the case of interest here, induced by a fan placed at the top of the tower. Considering the control volume shown in Fig. 2.1, the governing equations for the air temperature, T_a, water temperature, T_w, mass flow-rate of water, m_w, and relative humidity of air, ω, are derived following Klimanek and Bialecki's method [17].

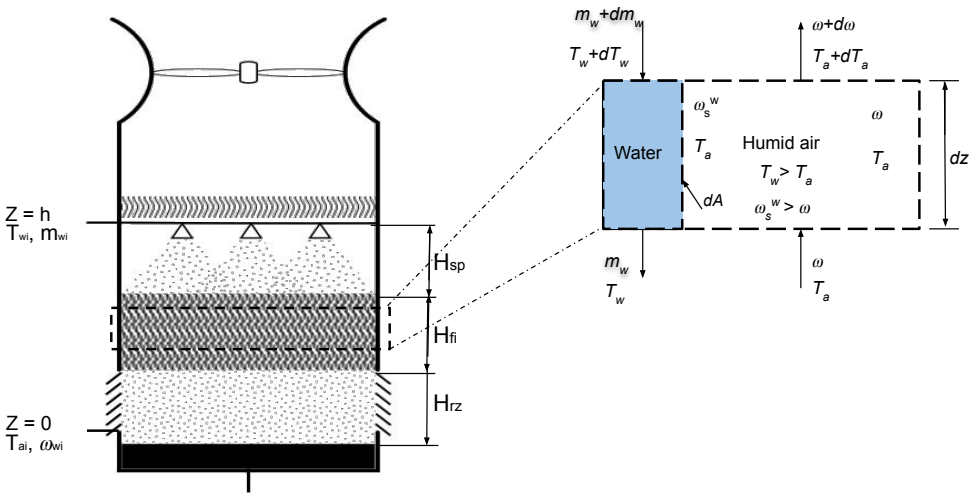

FIGURE 2.1: Control volume of a section of the fill in a wet cooling tower

2.2.1 Governing equations for unsaturated air

Applying a mass and energy balance to the control volume defined in Fig. 2.1 yields

$$\frac{\mathrm{d}m_w}{\mathrm{d}z} = m_a \frac{\mathrm{d}\omega}{\mathrm{d}z} \tag{2.1}$$

$$c_{pw}^w T_w \frac{\mathrm{d}m_w}{\mathrm{d}z} + m_w c_{pw}^w \frac{\mathrm{d}T_w}{\mathrm{d}z} = m_a \frac{\mathrm{d}h_a^a}{\mathrm{d}z} \tag{2.2}$$

respectively, where m_w is the mass flow rate of water, m_a is the mass flow rate of air, T_w is the water temperature, T_a is the air temperature, ω is the relative humidity of air, and c_{pw} is the specific heat capacity of water. The superscript 'w' indicates that the variable in question (here either c_{pw} or ω), and humidity, ω, will be evaluated at the bulk water temperature. Similarly, a superscript 'a' indicates that the variable in question will be will be evaluated at a bulk air temperature. Finally, h_a is the enthalpy of humid air per unit mass of dry air. For unsaturated air, h_a takes the form

$$h_a^a = c_{pa}^a T_a + \omega^a (r_0 + c_{pv}^a T_a) \tag{2.3}$$

where r_0 is the latent heat of vaporization evaluated at a reference temperature $T_w = 0°\mathrm{C}$. Moreover, c_{pv} and c_{pa} are the specific heat capacities measured at constant pressure for water-vapor and dry air.

The air at the air-water interface is assumed to be saturated, while the ambient air is unsaturated. This difference in saturation drives a transfer of water vapour from the interfacial region to the upflowing air. The rate of mass transfer at the air-water

interface is proportional to the difference in saturation between the air-water interface and the bulk air. The equation governing the kinetics of mass evaporation reads

$$\frac{\mathrm{d}m_w}{\mathrm{d}A} = \beta(\omega_s^w - \omega^a) \tag{2.4}$$

where β is the average mass transfer coefficient and ω_s^w is the relative humidity ratio of the saturated air at the air-water interface. The interfacial area is given by

$$\mathrm{d}A = a_f A_z \mathrm{d}z \tag{2.5}$$

where a_f is the transfer area per unit volume, A_z is the cross sectional area of the fill and $\mathrm{d}z$ is the small vertical distance defined in Fig. 2.1. Substituting (2.5) into (2.4) yields

$$\frac{\mathrm{d}m_w}{\mathrm{d}z} = \beta\, a_f\, A_z(\omega_s^w - \omega^a) \tag{2.6}$$

Combining this last result with (2.1) yields

$$\frac{\mathrm{d}\omega}{\mathrm{d}z} = \frac{\beta a_f A_z(\omega_s^w - \omega^a)}{m_a} \tag{2.7}$$

The total heat rejected by the water to the air can be expressed as the sum of latent heat, $\mathrm{d}Q_l$, and sensible heat, $\mathrm{d}Q_s$. Similar to (2.4), the latent heat transfer is given by

$$\mathrm{d}Q_l = h_e^w \mathrm{d}m_w = h_e^w \beta(\omega_s^w - \omega^a)\mathrm{d}A \tag{2.8}$$

where h_e^w is the enthalpy of the evaporating water evaluated at the bulk water temperature T_w, i.e.

$$h_e^w = r_0 + c_{pv}^w T_w \tag{2.9}$$

Meanwhile, and from Newton's law of cooling, the sensible heat transfer can be expressed as

$$\mathrm{d}Q_s = \alpha(T_w - T_a)\mathrm{d}A \tag{2.10}$$

where α is the heat transfer coefficient. Combining (2.8-2.10), the total heat transfer rate can be expressed as

$$\mathrm{d}Q = [h_e^w \beta(\omega_s^w - \omega^a) + \alpha(T_w - T_a)]\mathrm{d}A \tag{2.11}$$

At steady state, the energy transferred from the water to the air by latent and sensible effects must be balanced by the increase in the enthalpy of the air. In symbols, we

write

$$m_a \frac{\mathrm{d}h_a}{\mathrm{d}z} = [h_e^w \beta(\omega_s^w - \omega^a) + \alpha(T_w - T_a)] a_f A_z \tag{2.12}$$

Differentiating (2.3) with respect to the vertical coordinate allows us to compute the left-hand side derivative, i.e.

$$\frac{\mathrm{d}h_a}{\mathrm{d}z} = (c_{pa}^a + \omega^a c_{pv}^a)\frac{\mathrm{d}T_a}{\mathrm{d}z} + (r_0 + c_{pv}^a T_a)\frac{\mathrm{d}\omega}{\mathrm{d}z} \tag{2.13}$$

Combining (2.12) and (2.13), and using (2.5) and (2.7), allows us write a governing equation for the bulk air temperature, i.e.

$$\frac{\mathrm{d}T_a}{\mathrm{d}z} = \frac{\beta a_f A_z [\mathrm{Le}_f (T_w - T_a)(c_{pa}^a + \omega^a c_{pv}^a) + (c_{pv}^w T_w - c_{pv}^a T_a)(\omega_s^a - \omega^a)]}{m_a (c_{pa}^a + c_{pv}^a \omega^a)} \tag{2.14}$$

In like fashion, we can evaluate the spatial derivative of T_w by combining (2.2), (2.6) and (2.13), i.e.

$$\frac{\mathrm{d}T_w}{\mathrm{d}z} = \frac{\beta a_f A_z \left[\mathrm{Le_f} (T_w - T_a)(c_{pa}^a + \omega^a c_{pv}^a) + (r_0 + c_{pv}^w T_w - c_{pw}^w T_w)(\omega_s^a - \omega^a)\right]}{m_w c_{pw}^w} \tag{2.15}$$

The Lewis factor, Le_f, which appears in the governing equation has to evaluated to solve the set ODEs. The Lewis factor is a dimensionless number used to measure the relative rate of heat and mass transfer in a evaporative process. It is defined as the ratio of the heat transfer Stanton number to the mass transfer Stanton number. Expressed symbolically

$$\mathrm{Le}_f \equiv \frac{\mathrm{St}}{\mathrm{St}_m} = \frac{\alpha}{\beta(c_{pa}^a + \omega c_{pv}^a)} \tag{2.16}$$

Here, St and St_m are, respectively, the heat and mass transfer Stanton numbers. Evaluating the mass transfer coefficient β and heat transfer coefficient α can be an arduous process [17]. Bosnjakovic [27] developed an empirical relation for the Lewis factor for air-vapor systems as a function of humidity and saturation humidity ratio of air. For unsaturated air, his equation reads

$$\mathrm{Le}_f = 0.866^{2/3} \frac{\frac{\omega_s^w + 0.622}{\omega^a + 0.622} - 1}{\ln\left(\frac{\omega_s^w + 0.622}{\omega^a + 0.622}\right)} \tag{2.17}$$

The empirical relation developed by Bosnjakovic[27] as a function of humidity and saturation humidity ratio, avoids arduous calculation of heat transfer coefficient, α and mass transfer coefficient, β.

2.2.2 Governing equations for supersaturated air

When the rate of evaporation is large, the water content in the upflowing air gradually increases to the point of supersaturated conditions leading to the formation of fine water droplets or mist. The water in contact with such supersaturated air is cooled until the driving potential $\omega_s^w - \omega_s^a$ becomes positive (i.e. local water temperature is higher than the bulk air temperature) [17]. The equations outlined above must then be modified to capture the physics of supersaturated air e.g. (2.4) becomes

$$\frac{\mathrm{d}m_w}{\mathrm{d}A} = \beta(\omega_s^w - \omega_s^a) \tag{2.18}$$

Meanwhile the enthalpy and Lewis factor for supersaturated air are respectively evaluated from

$$h_{sat} = c_{pa}^a T_a + \omega_s^a(r_0 + c_{pv}^a T_a) + (\omega^a - \omega_s^a)c_{pw}^a T_a \tag{2.19}$$

$$\mathrm{Le_f} = 0.866^{2/3}\frac{\frac{\omega_s^w+0.622}{\omega_s^a+0.622} - 1}{\ln\left(\frac{\omega_s^w+0.622}{\omega_s^a+0.622}\right)} \tag{2.20}$$

Analogous to the procedure for unsaturated air, a set of ODEs are derived for supersaturated air. Complementing (2.6), (2.7), (2.14) and (2.15), these read as follows:

$$\frac{\mathrm{d}m_w}{\mathrm{d}z} = \beta a_f A_z(\omega_s^w - \omega_s^a) \tag{2.21}$$

$$\frac{\mathrm{d}\omega}{\mathrm{d}z} = \frac{\beta a_f A_z(\omega_s^w - \omega_s^a)}{m_a} \tag{2.22}$$

$$\begin{aligned}\frac{\mathrm{d}T_a}{\mathrm{d}z} = \frac{-\beta a_f A_z}{m_a}\Big[&\mathrm{Le_f}c_{pa}^a(T_w - T_a) - \omega_s^w(r_0 + c_{pv}^w T_w)\\ &+ c_{pw}^a(\mathrm{Le_f}(T_w - T_a)(\omega^a - \omega_s^a) + T_a(\omega_s^w - \omega_s^a))\\ &+ \omega_s^a(r_0 + c_{pv}^a \mathrm{Le_f}(T_a - T_w)) + c_{pv}^w T_w\Big]\\ &/\left[c_{pa}^a + c_{pw}^a\omega^a + \frac{\mathrm{d}\omega_s^a}{\mathrm{d}T_a}(r_0 + c_{pv}^a T_a - c_{pw}^a T_a) + \omega_s^a(c_{pv}^a - c_{pw}^a)\right]\end{aligned} \tag{2.23}$$

$$\frac{\mathrm{d}T_w}{\mathrm{d}z} = \frac{\beta a_f A_z[(r_0 + c_{pv}^w T_w - c_{pw}^w T_w)(\omega_s^w - \omega_s^a) + \mathrm{Le_f}(T_w - T_a)(c_{pa}^a + c_{pw}^a(\omega^a - \omega_s^a) + c_{pv}^a\omega_s^a)]}{m_w c_{pw}^w} \tag{2.24}$$

2.2.3 Merkel number calculation

Through the solution process, i.e. equations (2.6), (2.7), (2.14) and (2.15) for unsaturated air and (2.18-2.24) for supersaturated air, the triple product of $\beta a_f A_z$ has to be

evaluated. Typically, this product is incorporated into the definition of a Merkel number, Me, whose value is measured in experiments or else is provided by manufactures [22]. The relationship between $\beta a_f A_z$ and Me is given by

$$\beta a_f A_z = \frac{\mathrm{Me}\, m_w}{H} \tag{2.25}$$

where H is the height of the cooling tower zone in question.

The spray zone data represented by Lowe and Christie [28] was correlated by Kröger [4] to give a Merkel number for the spray zone as a function of the spray zone height, H_{sp}, and the mass velocity of air, G_a, and of water, G_w, i.e.

$$\mathrm{Me}_{sp} = 0.2 H_{sp} \left(\frac{G_a}{G_w} \right)^{0.5} \tag{2.26}$$

An alternative expression for Me_{sp} was developed by Reuter et al. [29] who chose to additionally represent the spray zone Merkel number as a function of the Sauter mean drop diameter, d, i.e.

$$\mathrm{Me}_{sp} = 7.465 \times 10^{-6}\, G_a^{0.11}\, G_w^{-0.04}\, d^{-1.38} \tag{2.27}$$

For our calculations, we do not make an a-priori assumption regarding the nozzle type or the characteristics (e.g. drop size distribution) of the resulting spray and so use (2.26) instead of (2.27).

The Merkel number for fill material is derived from laboratory fill performance tests. The coefficients for the empirical equations are reported in terms of dependent functions such as the mass velocity of air and water. A number of different formats for the associated empirical equation have appeared in the cooling tower literature. For example, Johnson [30] expressed the fill zone Merkel number as

$$\mathrm{Me}_{fi} = C_1\, H_{fi}^{C_2}\, G_w^{C_3}\, G_a^{C_4} \tag{2.28}$$

whereas Kloppers [31] considered instead an equation of the form

$$\mathrm{Me}_{fi} = H_{fi}(C_1 G_w^{C_2} G_a^{C_3} + C_4 G_w^{C_5} G_a^{C_6}) \tag{2.29}$$

Here H_{fi} is the height of fill zone and C_1 through C_6 are curve fitting constants associated with a specific fill [30].

De Villiers and Kröger [32] derived a series of equations to describe the heat and mass transfer in the rain zone considering a counter-flow cooling tower. In doing so, a number of simplifying assumptions were made, i.e., (i) there is no droplet agglomeration, (ii) the droplet diameter is constant, (iii) droplets have negligible velocity when they detach from the base of the fill, and (iv) droplet diameters, d_d, and fall velocities, $v_r z$, are small enough so that the velocity of the counter-flowing air is not perturbed. The rain zone Merkel number, Me_{rz}, is estimated by first considering the mass transfer coefficient for a single drop using the semi-empirical equation developed by Ranz and Marshall [33],

$$\mathrm{Sh} = \frac{\beta\, d_d}{D} = 2 + 0.6\,\mathrm{Re}^{0.5}\,\mathrm{Sc}^{0.33} \tag{2.30}$$

where Sh is a Sherwood number, defined as the ratio of the rate of convective mass transfer to the rate of diffusive mass transfer. Moreover, D, is the molecular diffusion coefficient. Finally, $\mathrm{Re} = \rho_a\, v_d\, d_d/\mu_a$ is the droplet Reynolds number and $\mathrm{Sc} = \mu_a/(\rho_a\, D)$ is the droplet Schmidt number in which ρ_a is the density of air, and μ_a is its dynamic viscosity. Muira et al. [34] show that the above correlation is valid up to a Reynolds number of 2000. Upon integration of all the drops over the height, H_{rz}, of the rain zone, and assuming a rectangular cooling tower of width W_{ct}, it can ultimately be shown that

$$\begin{aligned}
\mathrm{Me}_{rz} = \frac{3.6\, P_{ai}\, D\, H_{rz}\, \mathrm{Sc}^{0.33}}{R_v\, T_a\, \rho_w\, v_{rz}\, d_d^2} & \left[\ln\left(\frac{\omega_s + 0.622}{\omega + 0.622}\right)\frac{1}{\omega_s - \omega}\right] \\
& \Big(4.68851\, a_\rho\, \rho_{av} - 187128.7\, a_\mu\, \mu_{av} - 2.29322 + 22.411 \\
& \left[0.350396(a_v\, v_{rz})^{1.38046} + 0.09\right] \\
& \times \left[1.60934(a_L\, H_{rz})^{-1.12083} + 0.66\right] \\
& \times \left[34.6765(a_L\, d_d)^{0.732448} + 0.45\right] \\
& \times \exp\Big\{7.7389\exp(-0.399827\, a_L\, H_{rz}) \\
& \times \ln\left[0.087498\exp(0.05323\, a_L W_{ct}) + 0.85\right]\Big\}\Big)
\end{aligned} \tag{2.31}$$

where v_{rz} is the inlet air velocity in the rain zone, P_{ai} is the ambient pressure, and R_v is the gas constant. When, by contrast, the cooling tower is circular in cross-section,

(2.31) is modified to read

$$\begin{aligned}\mathrm{Me}_{rz} = \frac{12\,P_{ai}\,D\,H_{rz}\,\mathrm{Sc}^{0.33}}{R_v\,T_a\,\rho_w\,v_{rz}\,d_d^2}\left[\ln\left(\frac{\omega_s+0.622}{\omega+0.622}\right)\frac{1}{\omega_s-\omega}\right] \\ \times\{0.90757a_\rho\rho_{av,ai}-30341.04a_\mu\mu_{ai}-0.37564+4.04016 \\ \times((0.55+41.7215(a_Ld_d)^{0.80043}) \\ \times\left[0.713+3.741(a_LH_{rz})^{-1.23456}\right] \\ \times[3.11\exp(0.15a_vv_{rz})-3.13] \\ \times\exp\left[(5.3759\exp(-0.2092a_LH_{rz}))\right. \\ \left.\times\ln(0.3719\exp(0.003811a_LR_{ai})+0.55)\right]\}\end{aligned} \tag{2.32}$$

In these last two equations, the 'a' coefficients are obtained from ρ_w, σ_w and gravitational acceleration, g, i.e. $a_\mu = 3.06\times10^{-6}\,(\rho_w^4 g^9/\sigma_w)^{\frac{1}{4}}$, $a_\rho = 998/\rho_w$, $a_v = 73.298\,(g^5\sigma_w^3/\rho_w^3)^{\frac{1}{4}}$ and $a_L = 6.122\,(g\sigma_w/\rho_w)^{\frac{1}{4}}$. Finally, R_{ai} is the circular cooling tower radius.

2.2.4 Boundary condition and initial guess

In order to solve the nonlinear ODEs (2.6), (2.7), (2.14) and (2.15) and/or (2.18-2.24), four boundary conditions are required. Boundary conditions are specified at the air inlet/bottom of the rain zone ($z = 0$) where we prescribe properties (i.e. temperature, T_{ai} and humidity ratio, ω_{ai}) of the inflowing ambient air. Boundary conditions are also specified at the spray zone/water inlet ($z = H$) based on the heat load, i.e. the inlet water temperature, T_{wi}, and the mass flow rate of water, m_w. Expressed symbolically,

$$T_a(z=0) = T_{ai};\ \omega_a(z=0) = \omega_{ai} \tag{2.33}$$

$$T_w(z=H) = T_{wi};\ m_w(z=H) = m_{wi} \tag{2.34}$$

Because half of the boundary conditions are specified at $z = 0$ and the other half at $z = H$, we pursue an iterative method of solution involving specification of an initial guess. To this end, it is helpful to apply the following approximations, developed by Kloppers [35], for the water and air outlet temperatures:

$$T_{wo} \approx \frac{T_{wi}+2\,T_{wbai}+T_{ai}}{4} \tag{2.35}$$

$$T_{ao} \approx \frac{T_{wo}+T_{wi}}{2} \tag{2.36}$$

where T_{wbai} is the ambient wet-bulb temperature. Note that the relative humidity of the exiting air, ω_{ao}, can be approximated based on T_{ao}. In turn, the outlet water

flowrate, m_{wo}, can be estimated from

$$m_{wo} \approx m_{wi} - m_a(\omega_{ao} - \omega_{ai}) \tag{2.37}$$

In numerically solving the sets of ODEs (2.6 -2.7), (2.14 - 2.15) or (2.21-2.24), we recognize that an air stream that is initially unsaturated may become saturated somewhere within one of the rain, fill or spray zones. In this eventuality, tests are performed to check the whether the air is unsaturated ($\omega \leq \omega_a^s$) or super-saturated ($\omega > \omega_a^s$). Depending on the condition either equations for saturated air, (2.6 -2.7), (2.14 - 2.15) or supersaturate air (2.21-2.24) are invoked. Furthermore, an additional test is formed to check for the position of z, such that zone specific Merkel number can be invoked. To solve the above set of equations (2.6 -2.7), (2.14 - 2.15) or (2.21-2.24), a Python BVP solver, "solve_bvp" is used. The algorithm in question is a fourth order collocation routine based on residual and adaptive step size control [36].

2.3 Dry cooling

The dry section typically consists of air-cooled heat exchangers, where ambient air is blown across several bundles of finned tubes. Various techniques have been developed for designing heat exchanges; those based on the log mean temperature difference (LMTD) and e-NTU method are arguably the most popular [13]. In this work, an e-NTU model is employed in simulating thermodynamic properties of an air-cooled heat exchanger. Empirical correlations derived by Ganguli [37] and Pieter [2] are adapted to determine the heat transfer coefficients happening in a heat exchanges.

2.3.1 Air side heat transfer coefficient

To evaluate the air side heat transfer coefficient for a heat exchanger including finned tubes, we use a correlation proposed by Ganguli [37]. The Nusselt number, Nu_a, for the air flowing through a finned tube heat exchanger is given by

$$\mathrm{Nu}_a = 0.38\mathrm{Re}^{0.6}\mathrm{Pr}^{0.333}\left(\frac{A_a}{A_r}\right)^{-0.15} \tag{2.38}$$

where $\mathrm{Re} = \frac{\rho v_{ai}^{dry}}{\mu}$, is the Reynolds number, where ρ, μ, and v_{ai}^{dry} are the density, dynamic viscosity, and velocity of the inlet air vapor and d_r is the fin root diameter. Also, $\mathrm{Pr} = \frac{\mu c_{pv}^a}{k_a}$ is the Prandtl number, where k_a is the thermal conductivity of air.

Finally, A_a is the total air-side area, and A_r is the root area if no fins are present. The ratio of the total air-side area to the root mean area is given by

$$\frac{A_a}{A_r} = \frac{\left[\frac{d_f^2 - d_r^2}{2} + d_f t_{ft} + d_r(P_f - t_{fr})\right]}{d_r P_f} \tag{2.39}$$

where d_f, P_f, t_{fr}, and t_{ft} are, respectively, fin diameter, fin pitch, mean fin thickness, and fin tip thickness as shown in Figure 2.2.

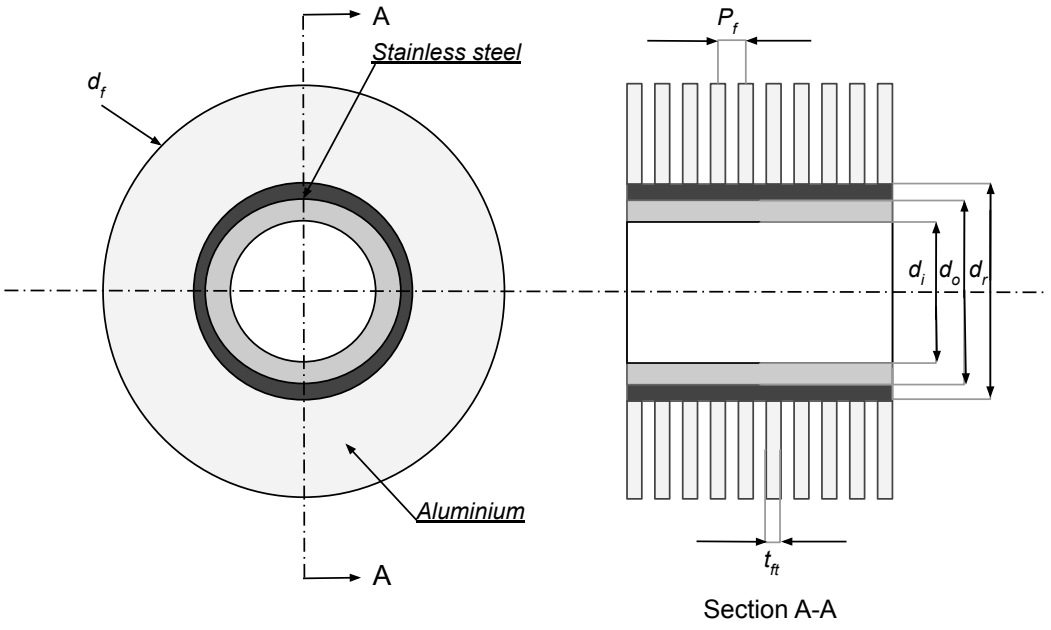

FIGURE 2.2: A schematic of extruded bi-metallic finned tube.

Equation 2.38 is valid for the following ranges: 11.17 mm $< d_r <$ 50.80 mm; 5.82 mm $< d_f - d_r <$ 19.05 mm; 2.3 mm $< p_f <$ 3.2 mm; 0.25 mm $< t_f <$ 0.56 mm; 27.43 mm $< P_t <$ 98.55 mm; 1800 $<$ Re $<$ 100,000; $1 < A_a/A_r < 50$.

Ganguli's correlation is helpful because it allows one to compute the air-side heat transfer coefficient using [37]

$$h_a = \frac{\mathrm{Nu}_a k_a}{d_r} \tag{2.40}$$

where k_a is the thermal conductivity of air. To evaluate the effective heat transfer coefficient, the air-side heat transfer coefficient,estimated from (2.40), has to be multiplied by the surface effectiveness, e_f

$$e_f = A_f \frac{1 - \eta_f}{A_a} \tag{2.41}$$

where η_f is the fin efficiency. For a radial fin of uniform thickness, η_f can be estimated from the empirical equation given by Schmidt [38], i.e.

$$\eta_f = \frac{\tanh\left(bd_r\frac{\phi}{2}\right)}{bd_r\frac{\phi}{2}} \tag{2.42}$$

where

$$b = \left(\frac{2h_a}{k_f t_f}\right)^{0.5}$$

In this last equation, k_f is the thermal conductivity of the material comprising the fin, t_f is the fin thickness and

$$\phi = \left(\frac{d_f}{d_r} - 1\right)\left[1 + 0.35\,\ln\left(\frac{d_f}{d_r}\right)\right]$$

With η_f to hand, the effective air-side heat transfer coefficient, h_{ae}, is given in terms of h_a by

$$h_{ae} = h_a e_f \tag{2.43}$$

2.3.2 Water side heat transfer coefficient

Heat transfer from the water to the interior pipe wall is determined by the nature of the liquid flow be it laminar, transitional, or turbulent. For most cases of industrial interest, it is appropriate to consider a turbulent flow [2]. In this case, the following correlation can be employed [37]:

$$\mathrm{Nu}_w = \frac{(f_D/8)(\mathrm{Re} - 1000)\,\mathrm{Pr}\left[1 + (d/L)^{0.67}\right]}{1 + 12.7(f_D/8)^{0.5}(\mathrm{Pr}^{0.67} - 1)} \tag{2.44}$$

where f_d is the friction factor. For a smooth tube, the friction factor is given by

$$f_d = (1.82\log_{10}\mathrm{Re} - 1.62)^{-2} \tag{2.45}$$

Equation (2.44) is valid provided, $2300 < \mathrm{Re} < 10^6$; $0.5 < \mathrm{Pr} < 10^4$; and $0 < d/L < 1$. The corresponding water side heat transfer coefficient is calculated using

$$h_w = \frac{\mathrm{Nu}_w k_w}{d_i} \tag{2.46}$$

where d_i is the inner diameter of the tube and k_w is the thermal conductivity of water. For a single pass heat exchanger in a crossflow configuration, as shown in Figure 2.3, the effectiveness is given by [39]

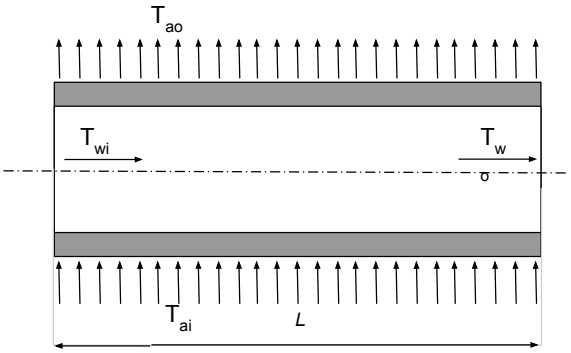

FIGURE 2.3: Schematic of a fluid flow direction in a single pass heat exchanger in a crossflow configuration.

$$e = \frac{1 - \exp[\mathrm{NTU}^{0.22}(\exp\left(-C\,\mathrm{NTU}^{0.78}\right) - 1)]}{C} \tag{2.47}$$

The effectiveness of the heat exchanger, e, is defined as the ratio of the actual heat transfer, Q_d, to the maximum (theoretical) heat transfer. Expressed symbolically

$$e = \frac{Q_d}{Q_{max}} \tag{2.48}$$

For a heat exchanger with four or more passes, the effectiveness can be determined using the crossflow equation given by Holman [39]

$$e = \frac{1 - \exp[-\mathrm{NTU}(1 - C)]}{1 - C\exp[-\mathrm{NTU}(1 - C)]} \tag{2.49}$$

where $C = \frac{C_{min}}{C_{max}}$ is the heat capacity ratio and $\mathrm{NTU} = \frac{UA}{C_{min}}$ is the number of transfer units. In these latter two equations, C_{min} is the minimum heat capacity ratio between the two fluids (water and air). Meanwhile, U is the overall heat transfer coefficient accounting for thermal resistance due to convection as well as conduction; it is given by

$$\frac{1}{U} = \left[\frac{1}{h_w} + \frac{A_w \ln(d_o/d_i)}{2\pi k_f L_t n_r n_{tr} n_b} + \frac{A_w}{A_a h_a}\right] \tag{2.50}$$

where A_w is the total surface area of the tube (water-side), d_o is the outside diameter of the tube, k_t is the thermal coefficient of the fin, n_{tr} is the number of tube per row, n_r is the number of tube rows, n_b is the number of heat exchanger bundles, and L_t is

the tube length. The actual heat transfer in a heat exchanger is evaluated using (2.48)

$$Q_d = e\, Q_{max} \tag{2.51}$$

where $Q_{max} = \min\{c_{pw}, c_{pa}\}(T_{wi} - T_{ai})$ is the maximum theoretical heat transfer rate in a heat exchanger. From (2.51), the water and air outlet temperatures from the dry section can be calculated from

$$T_{wo} = T_{wi} - \frac{Q_d}{c_{pw} m_w} \tag{2.52}$$

$$T_{ao} = T_{ai} + \frac{Q_d}{c_{pa} m_a} \tag{2.53}$$

2.4 Plenum chamber

To predict the temperature and humidity of the air leaving a hybrid cooling tower, one must perform a mass and energy balance on the plenum chamber. In so doing, one must account for the air streams emanating from the wet and dry sections of the tower. As suggested by the flowchart of Figure 2.4, these are mixed in the plenum chamber and thereafter discharged to the atmosphere. Assuming complete (100%) mixing in plenum chamber, the humidity of this exiting air stream can be computed from

$$\omega_{out} = \frac{m_{ai}^{wet} \omega_{ao}^{wet} + m_{ai}^{dry} \omega_{ai}}{m_{ai}^{wet} + m_{ai}^{dry}} \tag{2.54}$$

where m_{ai}^{wet} and m_{ai}^{dry} are, respectively, the mass flow rates of air entering the wet and dry sections of the cooling tower, and ω_{ao}^{wet} is the relative humidity ratio of the air exiting the wet section. Finally, the outlet air temperature, T_{ao}, from a cooling tower is evaluated from

$$T_{ao} = \frac{m_{ai}^{dry} h_{ao}^{dry} + m_{ai}^{wet} h_{ao}^{wet}}{m_{pc} c_{pw}} - \frac{r_0}{c_{pw}} \tag{2.55}$$

where h_{ao}^{dry}, h_{ao}^{wet}, and h_{pc} are, respectively, the enthalpies of the air at the outlets of the dry section, the wet section and the tower, and m_{pc} is the total air flow rate as measured in the plenum chamber. This latter quantity can be evaluated from

$$m_{pc} = m_{ao}^{wet}(1 + \omega_{ao}^{wet}) + m_{ai}^{dry}(1 + \omega_{ai}) \tag{2.56}$$

The temperature, humidity and velocity of the air leaving the cooling tower are used in specifying source conditions for the resulting atmospheric plume. In turn, it is

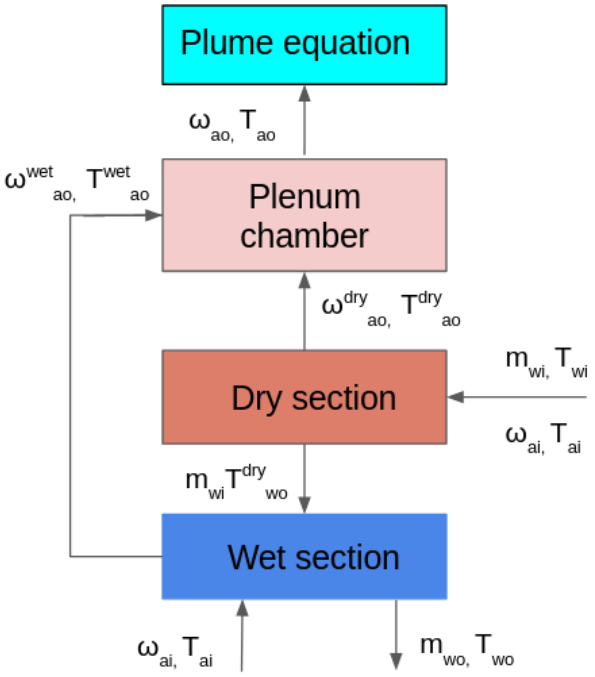

FIGURE 2.4: Flowchart representing the input variables required for solving a wet-dry augmented model

necessary to review the equations describing the evolution of this plume in physical and thermodynamic space. This is the subject of the next chapter.

Chapter 3

Turbulent plume model

3.1 Introduction

In this chapter, we derive the governing equations for a turbulent plume in a uniform ambient. The detailed derivation of the governing equations is presented in subsections 3.2.1, 3.2.2, and 3.2.3. Boundary conditions and merging criteria (in the case of multiple plumes) are also discussed in the later part of this chapter.

3.2 Governing equations

The plume solution is adapted from the work of Wu and Koh [1], which is a steady-state model that adds plume merger (among other details) to Morton's [40] seminal analysis of atmospheric plumes. The integral plume model in question is based on the conservation of mass, momentum, energy, and moisture. Wu and Koh's [1] model predicts plume properties such as temperature, humidity, velocity, and visible plume height. The model is based on the following assumptions:

1. Plumes emerging from the tower are considered axisymmetric and move vertically upwards, i.e. unlike [24] we do not consider the impact of wind forcing.
2. The pressure within the plume is hydrostatic.
3. The model output is independent of the Reynolds number as molecular transport is assumed negligible in comparison with turbulent transport.
4. The variation of density within the plume is small, i.e. less than 10%, so that the Boussinesq approximation can be applied.

5. The plume is considered to be relatively thin so that the boundary-layer approximation can employed.

6. Plume variables such as temperature, specific humidity, liquid moisture, and vertical velocity exhibit a “top-hat" profile that is self-similar in nature.

7. The ambient temperature and humidity are assumed independent of elevation; the ambient does not contain liquid moisture.

3.2.1 Volume flux

At any point within the plume, we require that the mass conservation equation be satisfied. This equation reads

$$\frac{\partial \rho}{\partial t} + \frac{1}{r}\frac{\partial}{\partial r}(r\rho u) + \frac{1}{r}\frac{\partial}{\partial \theta}(\rho v) + \frac{\partial}{\partial z}(\rho w) = 0 \tag{3.1}$$

where ρ is the fluid density and u, v, and w represent the velocity components in the radial, tangential, and vertical directions. Assuming a statistically steady and axisymmetric flow, the first and third terms on the left-hand side of (3.1) can be neglected, so that

$$\frac{1}{r}\frac{\partial}{\partial r}(r\rho u) + \frac{\partial}{\partial z}(\rho w) = 0 \tag{3.2}$$

This result is further simplified using the Boussinesq approximation. The approximation states that small density variations can be neglected except where density differences are multiplied with gravitational acceleration. On this basis, (3.2) reduces to

$$\frac{1}{r}\frac{\partial}{\partial r}(ru) + \frac{\partial w}{\partial z} = 0 \tag{3.3}$$

Multiplying (3.3) with $2\pi r$ and integrating from $r = 0$ to $r = \infty$ yields

$$\frac{\mathrm{d}}{\mathrm{d}z}\int_0^\infty 2\pi w r \mathrm{d}r = -2\pi \int_0^\infty \frac{\partial}{\partial r}(ru)\mathrm{d}r \tag{3.4}$$

$$\implies \frac{\mathrm{d}}{\mathrm{d}z}\int_0^\infty 2\pi r w \mathrm{d}r = -[2\pi r u]_0^\infty \tag{3.5}$$

The integral on the left-hand side of (3.4) represents the plume volume flux, Q. In the limiting case of $r \to \infty$, u approaches zero and the right-hand side product ru remains finite [23]. The product ru whether evaluated in the far or near field represents the entrainment of ambient fluid into the plume, as shown in Figure 3.1. The flow from infinity is driven by entrainment at the edges of the plume. From Taylor's entrainment hypothesis for an unstratified ambient, the entrainment velocity at the plume edge is

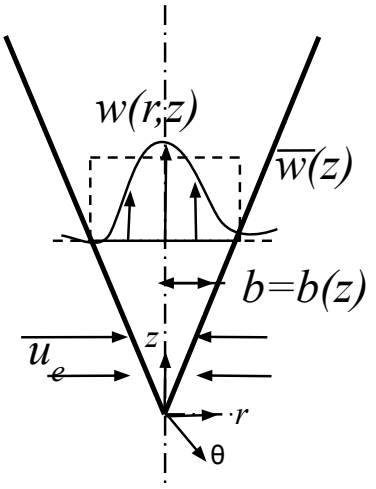

FIGURE 3.1: Schematic of an axisymmetric plume. $b(z)$ is the plume radius and $w(z)$ is the mean vertical velocity assuming a top-hat profile.

proportional to the mean vertical velocity [40]. Considering a "top-hat" profile for the plume vertical velocity (assumption 6), the entrainment velocity, u_e, can be expressed as

$$u_e = \gamma w \tag{3.6}$$

where γ is the entrainment coefficient, which takes the value of 0.117 for axisymmetric plumes [23]. Applying Taylor's entrainment hypothesis in (1.4) yields, after some simplification

$$\frac{\mathrm{d}Q}{\mathrm{d}z} = 2\pi b u_e \tag{3.7}$$

where b is the top-hat radius of the plume and u_e is the entrainment velocity, which varies as a linear function of z. Also, $Q = \int_0^\infty 2\pi w r \mathrm{d}r$ is defined as the volume flux.

3.2.2 Momentum flux

The Navier-Stokes equations of motion for a fluid in a cylindrical coordinate system are given by

$$\frac{\mathrm{D}u}{\mathrm{D}t} - \frac{v^2}{r} = -\frac{1}{\rho_o}\frac{\partial P}{\partial r} + \nu\left(\nabla^2 u - \frac{u}{r^2} - \frac{2}{r^2}\frac{\partial v}{\partial \theta}\right) \tag{3.8}$$

$$\frac{\mathrm{D}v}{\mathrm{D}t} - \frac{uv}{r} = -\frac{1}{\rho_o r}\frac{\partial P}{\partial \theta} + \nu\left(\nabla^2 v - \frac{v}{r^2} + \frac{2}{r^2}\frac{\partial u}{\partial \theta}\right) \tag{3.9}$$

$$\frac{\mathrm{D}w}{\mathrm{D}t} = -\frac{g\rho}{\rho_o} - \frac{1}{\rho_o}\frac{\partial P}{\partial z} + \nu\nabla^2 w \tag{3.10}$$

For an axisymmetric plume $v = 0$, and $\frac{\partial}{\partial\theta} = 0$ [41]. The governing equations can be further simplified by assuming the plume to be relatively thin so that a boundary-layer approximation can be invoked. In this case, and with the exception of pressure, derivatives with respect to r are much larger than those with respect to z, i.e. $\frac{\partial}{\partial r} \gg \frac{\partial}{\partial z}$. Equations (3.8), (3.9) and (3.10) can then be written as

$$u\frac{\partial w}{\partial r} + w\frac{\partial w}{\partial z} = -\frac{1}{\rho_o}\frac{\partial P}{\partial r} \tag{3.11}$$

$$0 = -\frac{1}{\rho_o r}\frac{\partial P}{\partial \theta} \tag{3.12}$$

$$u\frac{\partial w}{\partial r} + w\frac{\partial w}{\partial z} = -\frac{\rho g}{\rho_o} - \frac{1}{\rho_o}\frac{\partial P}{\partial z} \tag{3.13}$$

By applying scaling analysis on (3.3) it can be shown that

$$\frac{u}{b} \sim \frac{w}{L} \tag{3.14}$$

where L is a characteristic length scale in z; by default, we assume that $L \gg b$. From (3.14) it can be shown that $w \sim uz/b$ and applying scaling analysis to (3.11) and (3.13) yields

$$\frac{u^2}{b} \sim \frac{1}{\rho_o}\frac{\partial P}{\partial r} \tag{3.15}$$

$$\left(\frac{u^2}{b}\right)\left(\frac{z}{b}\right) \sim \frac{1}{\rho_o}\frac{\partial P}{\partial z} + \frac{\rho g}{\rho_o} \tag{3.16}$$

from (3.15) and (3.16) it can be shown that

$$\left(\frac{\partial z}{\partial P}\right)\left(\frac{\partial P}{\partial r}\right) \sim \left(\frac{b}{z}\right) \ll 1 \tag{3.17}$$

Equation (3.17) implies that $\partial p/\partial z$ is much larger than $\partial p/\partial r$ i.e. pressure varies more rapidly with z than it does with r. Therefore, the pressure within the plume can, at leading order, be equated to the hydrostatic ambient pressure. The hydrostatic pressure relation is given by

$$\frac{\partial P}{\partial z} = -g\rho_a \tag{3.18}$$

where ρ_a is the ambient density. On substituting (3.18) into (3.13) and further simplifying, we obtain

$$u\frac{\partial w}{\partial r} + w\frac{\partial w}{\partial z} = \frac{g}{\rho_o}(\rho_a - \rho) = g' \tag{3.19}$$

where g' is the reduced gravity. Multiplying (3.19) with $2\pi r$ and integrating from $r = 0$ to $r = \infty$ yields

$$\int_0^\infty 2\pi r \left(u\frac{\partial w}{\partial z} + w\frac{\partial w}{\partial z} \right) \mathrm{d}r = \int_0^\infty 2\pi r g' \mathrm{d}r \tag{3.20}$$

Integrating (3.20) by parts and using (3.3), we obtain

$$\int_0^\infty 2\pi r u \frac{\partial w}{\partial r} \mathrm{d}r = [2\pi r u w]_0^\infty - \int_0^\infty 2\pi w \frac{\partial (ru)}{\partial r} \mathrm{d}r \tag{3.21}$$

Upon further simplification it can be shown that

$$\frac{\mathrm{d}M}{\mathrm{d}z} = 2\pi \int_0^\infty r g \frac{\rho_a - \rho}{\rho_o} \mathrm{d}r \tag{3.22}$$

Equation (3.22) can also be written as

$$\frac{\mathrm{d}M}{\mathrm{d}z} = g' \frac{Q^2}{M} \tag{3.23}$$

where $M = \int_0^\infty 2\pi r w^2 \, \mathrm{d}r$ is the momentum flux.

3.2.3 Conservation of heat and humidity

The scalar conservation equation assuming no sources, sinks or chemical reaction reads

$$\frac{\mathrm{D}c}{\mathrm{D}t} = \kappa \nabla^2 c \tag{3.24}$$

where c represents the scalar concentration. In the context of cooling tower plumes c denotes either temperature or moisture. Expanding (3.24), and assuming a steady flow, we write

$$\frac{1}{r}\frac{\partial (ruc)}{\partial r} + \frac{\partial (wc)}{\partial z} = \kappa \left[\frac{1}{r}\frac{\partial}{\partial r}\left(r\frac{\partial c}{\partial r} \right) + \frac{\partial^2 c}{\partial z^2} \right] \tag{3.25}$$

Because molecular diffusion is small compared to turbulent transport, and the turbulent flux is only a small fraction of the mean flux [42], we can neglect the diffusion term on the right-hand side of (3.25). The scalar transport equation can then be rewritten as

$$\frac{1}{r}\frac{\partial (ruc)}{\partial r} + \frac{\partial (wc)}{\partial z} = 0 \tag{3.26}$$

Multiplying (3.26) with $2\pi r$ and integrating from $r = 0$ to $r = \infty$ yields

$$2\pi \int_0^\infty \frac{\partial(rwc)}{\partial z}\mathrm{d}r + 2\pi \int_0^\infty \frac{\partial(ruc)}{\partial r}\mathrm{d}r = 0 \tag{3.27}$$

and therefore

$$\frac{\mathrm{d}}{\mathrm{d}z}\int_0^\infty 2\pi rwc\mathrm{d}r = -\lim_{r\to\infty}[2\pi ruc] \tag{3.28}$$

We consider the ambient scalar concentration, c_a, to vary with elevation, i.e. $c_a = c_a(z)$. Multiplying both sides of (3.3) by $2\pi r c_a$ and integrating from $r = 0$ to ∞ yields

$$\int_0^\infty 2\pi c_a \frac{\partial(ru)}{\partial r}\mathrm{d}r + \int_0^\infty 2\pi r c_a \frac{\partial w}{\partial z}\mathrm{d}r = 0 \tag{3.29}$$

Using integration by parts, (3.29) can be rewritten as

$$\frac{\mathrm{d}}{\mathrm{d}z}\int_0^\infty 2\pi r c_a w\mathrm{d}r = -\lim_{r\to\infty}[2\pi r c_a u] - \frac{\mathrm{d}c_a}{\mathrm{d}z}\int_0^\infty 2\pi rw\mathrm{d}r \tag{3.30}$$

Subtracting (3.30) from (3.28) yields

$$\frac{\mathrm{d}}{\mathrm{d}z}\int_0^\infty 2\pi rw(c-c_a)\mathrm{d}r = -\lim_{r\to\infty}[2\pi ru(c-c_a)] + \frac{\mathrm{d}c_a}{\mathrm{d}z}\int_0^\infty 2\pi rw\mathrm{d}r \tag{3.31}$$

As $r \to \infty$, $u \to 0$ and $c - c_a \to 0$. Hence (3.31) can be further simplified as

$$\frac{\mathrm{d}}{\mathrm{d}z}\int_0^\infty 2\pi rw(c-c_a)\mathrm{d}r = \frac{\mathrm{d}c_a}{\mathrm{d}z}\int_0^\infty 2\pi rw\mathrm{d}r \tag{3.32}$$

For a uniform ambient $\frac{\mathrm{d}c_a}{\mathrm{d}z} = 0$.

For cooling tower plumes, we consider the conservation of moisture and thermal energy separately. In the latter case, we need to account for the release of latent heat during condensation, and the resulting equation reads

$$\frac{\mathrm{d}}{\mathrm{d}z}\int_0^\infty 2\pi rw\left[(T_p - T_a) - \frac{r_0}{c_{pa}}\sigma\right]\mathrm{d}r = 0 \tag{3.33}$$

where T_p and T_a are, respectively, the temperature of the plume and of the ambient both measured in Kelvin, σ is the plume specific liquid moisture, r_o is the latent heat of vaporization, and c_{pa} is the specific heat of air at constant pressure. The temperature of ambient air, T_a, is assumed independent of elevation (assumption 7). Defining $\Theta = \int_0^\infty 2\pi rw(T_p - T_a)\mathrm{d}r$ and $W = \int_0^\infty 2\pi rw\sigma\mathrm{d}r$ as the mean temperature deficiency and specific liquid moisture flux, respectively, the thermal energy conservation equation is given by

$$\frac{\mathrm{d}}{\mathrm{d}z}\left(\Theta - \frac{r_o}{c_{pa}}W\right) = 0 \tag{3.34}$$

Complementing (3.34), the evolution equation for plume moisture is given by

$$\frac{\mathrm{d}}{\mathrm{d}z}\int_0^\infty 2\pi r w\left[(\omega_p-\omega_a)+\sigma\right]\mathrm{d}r=0 \tag{3.35}$$

where ω_p and ω_a are, respectively, the specific humidity of the plume and of the ambient. From assumption 7, the ambient specific humidity is presumed independent of z. Defining the specific humidity flux as $H=\int_0^\infty 2\pi r w(\omega_p-\omega_a)\mathrm{d}r$, moisture conservation is expressed as

$$\frac{\mathrm{d}}{\mathrm{d}z}(H+W)=0 \tag{3.36}$$

Summarizing the above derivations, the evolution equations that define the vertical variation of the plume volume flux, Q, momentum flux, M, temperature deficiency flux, Θ, specific humidity flux, H, and specific liquid moisture deficiency flux, W, read as follows:

$$\frac{\mathrm{d}Q}{\mathrm{d}z}=2\pi^{1/2}\gamma M^{1/2} \tag{3.37}$$

$$\frac{\mathrm{d}M}{\mathrm{d}z}=\frac{g'Q^2}{M} \tag{3.38}$$

$$\frac{\mathrm{d}}{\mathrm{d}z}\left(\Theta-\frac{r_o}{c_{pa}}W\right)=0 \tag{3.39}$$

$$\frac{\mathrm{d}}{\mathrm{d}z}(H+W)=0 \tag{3.40}$$

where γ is the entrainment coefficient, it takes a value of $\gamma_r=0.147$ and $\gamma_l=0.117$ for a line plume. Finally, g' is the reduced gravity and is given by

$$g^{'}=g\left(\frac{\rho_a-\rho}{\rho_a}\right)=g\left(1-\frac{T_{v,a}}{T_{v,p}}\right) \tag{3.41}$$

here $T_{v,a}$ and $T_{v,p}$ denote, respectively, the virtual temperature of the plume and of the ambient. The virtual temperature corresponds to the temperature of dry air having the same density as that of moist air at an identical pressure [43]. To account for condensation, we adopt a limiting case of foggy air where the liquid moisture content, σ, is zero. The equation presented by Emanuel [44] reads

$$T_{v,a}=T_a(1+0.608\omega_a) \tag{3.42}$$

By contrast, the plume virtual temperature, $T_{v,p}$, is given by

$$T_{v,p} = \left(T_a + \frac{\Theta}{Q}\right)\left[1 + 0.608\left(\omega_a + \frac{H}{Q}\right) - \frac{W}{Q}\right] \tag{3.43}$$

Equations (3.37 - 3.40) constitute four ODEs in five unknowns; the extra condition for model closure is given by

$$\begin{aligned} \sigma_p &= 0; \quad \text{for} \quad \omega_p < \omega_{sat} \quad \text{(dry plume)} \\ \sigma_p &= \omega_{sat}(T_a, P); \quad \text{for} \quad \omega_p \geq \omega_{sat} \quad \text{(wet plume)} \end{aligned} \tag{3.44}$$

Equation (3.44) implies that when the plume is subsaturated, the flux, W, of liquid moisture due to condensation is zero. When the plume is saturated, the plume humidity is equal to the plume saturation humidity.

Complementing the above evolution equations, a pressure term is introduced that varies hydrostatically with height, z, (assumption 2). To wit,

$$P = P_{amb} - \rho_p g z \tag{3.45}$$

where P is the pressure measured at arbitrary elevation, P_{amb} is the ambient pressure, and ρ_p is the plume density.

3.2.4 Input conditions for the plume model

After estimating, from the analysis of Chapter 2, the amount of heat and moisture that is absorbed by the stream of air that flows upwards through the cooling tower, we can determine conditions at the exit of the tower/base of the atmospheric plume. The boundary conditions required to solve the plume equations are

$$Q_0 = U_o A_o \tag{3.46}$$

$$M_0 = U_o^2 A_o \tag{3.47}$$

$$\left(\Theta_0 - \frac{r_o}{c_{pa}} W_0\right) = U_o A_o (T_a - T_p) \tag{3.48}$$

$$H_0 + W_0 = U_o A_o (\omega_a - \omega_p) \tag{3.49}$$

where the subscript $'0'$ represents a value that is measured at the plume source. The plume source velocity, U_o, is calculated from $U_o = \frac{m_a}{\rho A_o}$, where ρ is the moist air density, and the source area, A_o, is estimated from the inner diameter of the fan shroud. Starting

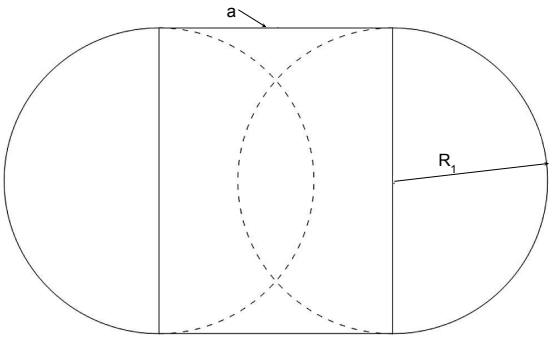

FIGURE 3.2: Cross-sectional view of plume merger [1]

from the above source conditions, the evolution equations (3.37 -3.40) are integrated in z up to some prescribed elevation using Python's "odelay" function.

3.2.5 Merging Criteria

The use of multiple cooling tower cells are a common means of waste heat disposal for large thermal loads. Due to the close proximity of cooling tower cells, the individual plume from one cooling tower cell is expected to interact with the plumes generated by adjacent cells. Consequently, we expect there to be an evolution of the composite plume shape as constituent plumes grow and merge. Typically, merging of the plume happens within a short vertical distance from the cooling tower exit (plume source).

According to Wu & Koh [45], plume merger is said to occur when the area of rectangle illustrated in figure 3.2 is equal to the area of the two semi-circles at the two ends. Upon merging, the entrainment functions are altered due to the change in plume shape i.e. from a round plume to line plume that includes a half-round plume at either end. For a merged plume, the cross-sectional area, A_l (A_r), and entrainment rate, E_l (E_r), for a half round (line) plume are respectively given by

$$\begin{aligned} A_l &= 2aR_1 \quad , E_l = 2\gamma_l aU \\ A_r &= \frac{1}{2}\pi R_1^2 \quad , E_r = \gamma_r \pi R_1 U \end{aligned} \tag{3.50}$$

Here, R_1 is the plume radius as measured at an elevation of merger, $a = \frac{\pi R_1}{2}$ is the center-to-center distance between the two merged plumes –see Figure 3.2. Finally, $\gamma_l = 0.147$ and $\gamma_r = 0.117$ are the entrainment coefficients for a line and a round plume, respectively [1]. After plume merger, the calculation of the two half round plumes and of the line plumes follows (3.37 - 3.40), by using E_r and E_l for a round plume and a line plume, respectively.

Chapter 4

Results and Discussion

4.1 Validation

4.1.1 Fill model

The developed model of section 2.1 has been validated against a numerical example from Klimanek [46]. The analysis was performed for a film type fill of height 1.2 m and a cross sectional area of 1 m^2. Input conditions are given in Table 4.1 and the Merkel number for the fill is given by [17]

$$\frac{\mathrm{Me}_{fi}}{H_{fi}} = 1.3805\, m_w^{0.1127}\, m_a^{0.6982} - 0.5170\, m_w^{0.4610}\, m_a^{0.6812} \tag{4.1}$$

Figure 4.1A and 4.1B indicate that the results obtained from the augmented model match well with Klimanek's [46] results. This confirms the accuracy of our solution, the calculation of which took less than a minute on a Intel® Core™ i7 computer.

TABLE 4.1: Input variables for the example of sub-section 4.1.1 [46].

Input variables	
Water inlet temperature, T_{wi} (K)	310.15
Water mass flow rate, m_w (kg/s)	3.00
Air inlet temperature, T_{ai} (K)	293.15
Inlet relative humidity, X_{ai} (kg/kg)	0.012
Ambient pressure, P_{ai} (Pa)	101,712.27
Air mass flow rate of air, m_a (kg/s)	3.00

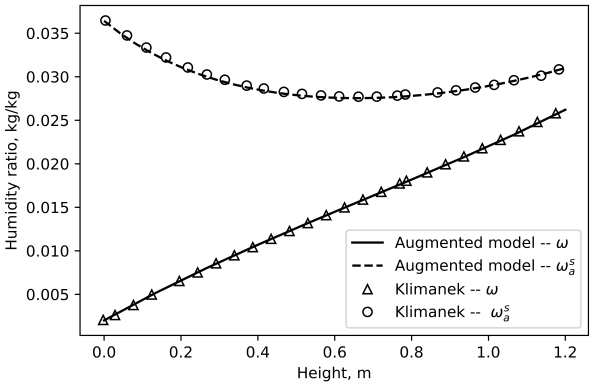

A Distribution of humidity and saturation humidity in the fill

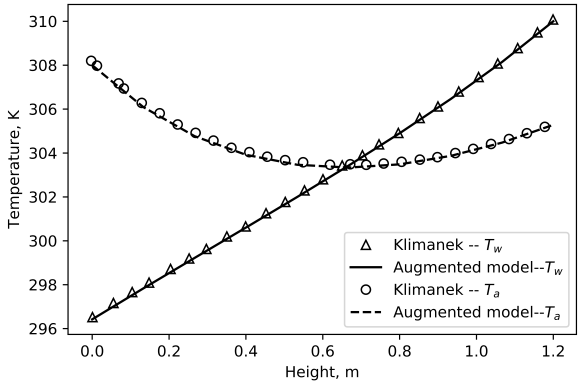

B Distribution of water and air temperature in the fill

FIGURE 4.1: Model output comparison between the augmented model of sub-section 4.1.1 and the Klimanek method [46]. In both of the above plots $z = 0\,\mathrm{m}$ and $z = 1.2\,\mathrm{m}$ correspond, respectively, to the base and top of the fill.

4.1.2 Comparison with the Poppe and Merkel methods

The augmented model is also compared with analogue solutions derived using the Poppe method [16] and the Merkel method [14]. The input variables for the numerical example are given in Table 4.2. In turn, we compare the results obtained from Merkel, Poppe and the augmented model in Table 4.3. The (minor) discrepancy between our augmented model vs. that of Poppe is explained chiefly by the different empirical functions applied in specifying the specific heats and the saturation pressures. The larger discrepancy with the output of the Merkel model is due to simplifying assumptions of Merkel's. Figure 4.2A, 4.2B respectively show the variation of key thermodynamic properties in the rain (rz), fill (fi), and spray (sp) zones obtained from solving the augmented model. The results in question show a good agreement with the lumped analysis of Klimanek and Bialecki [17]. The discrepancy seen in Figure 4.2A, 4.2B is because,

unlike Klimanek and Bialecki [17], the augmented model considers zone specific Merkel number.

TABLE 4.2: Input variables for the example of sub-section 3.2

Tower parameters	
Water inlet temperature, T_{wi} (K)	313.15
Water mass flow rate, m_w (kg/s)	12,500
Air inlet temperature, T_{ai} (K)	288.60
Inlet air wet bulb temperature, T_{wbai} (K)	284.20
Ambient pressure, P_{ai} (Pa)	84,100
Air mass flow rate, m_a (kg/s)	16,672.20
Rain zone height, H_{rz} (m)	10.00
Fill zone height, H_{fi} (m)	2.50
Spray zone height, H_{sp} (m)	0.50
Tower radius, R_{ct} (m)	52.25

TABLE 4.3: Comparison of results obtained using the Poppe and Merkel methods vs. the augmented model

	Augmented model	**Poppe method [22]**	**Merkel method**	**Absolute error, (vs. Poppe)**	**Absolute error, (vs. Merkel)**
T_{wo} (K)	294.41	294.56	294.63	0.15	0.22
T_{ao} (K)	299.95	299.86	299.15	0.09	0.80
ω_{ao} (kg/kg)	0.02781	0.02789	0.02699	0.00008	0.00082
ω_a^s (kg/kg)	0.02734	0.02718	0.02699	0.00016	00035
m_{wo} (kg/s)	12,171.94	12,170.50	12,500.00	1.44	328.06
Q (MW)	1011.00	1003.47	966.83	7.53	44.17

4.1.3 Comparison with experimental field data

The augmented model is further validated by drawing a comparison against data collected during a performance test conducted by International Cooling Tower, Inc. on a cooling tower installation located in Colorado. Tests were performed in August 2015. Three 1 hr long data sets were collected beginning at 10:20, 13:00 and 15:15 local time. Measurements were made on a ten cell rectangular counterflow cooling tower, parameters for which are given in Table 4.4. The cooling towers contained a film-type fill (OF21MA). Hot and cold water temperatures were respectively measured using three and four four-wire resistance-type temperature sensors. Table 4.5 presents the outlet water temperature obtained from the augmented model together with analogue field data. Encouragingly, errors are all within 0.2%.

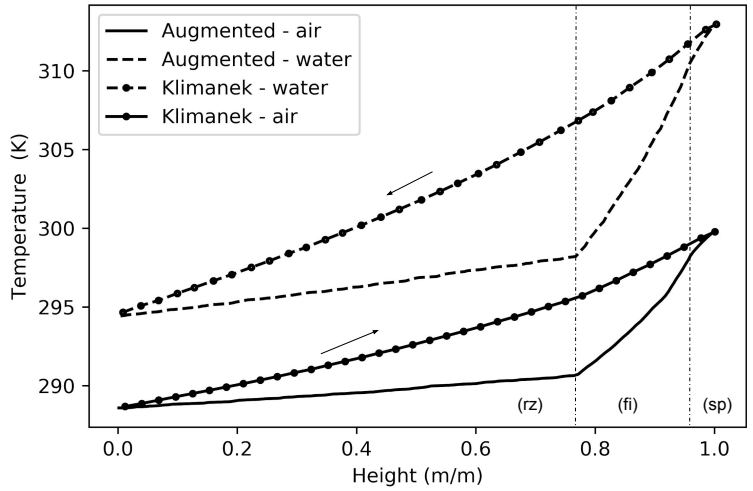

A Distribution of water and air temperature

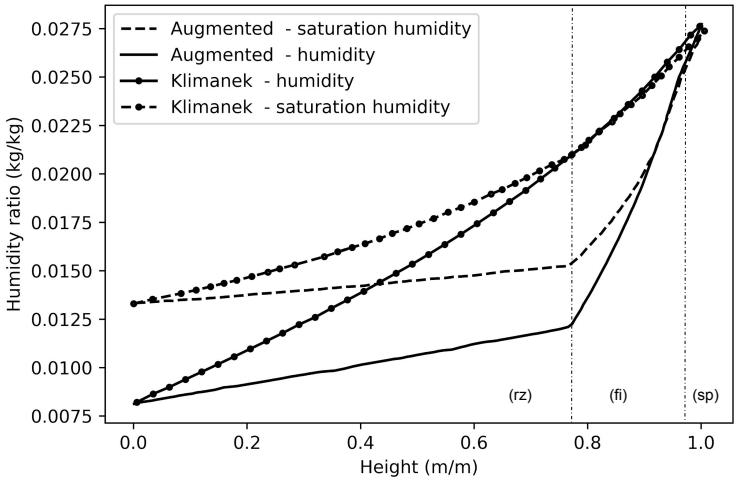

B Distribution of relative humidity and saturation humidity ratio

FIGURE 4.2: Model output comparison of temperature and humidity obtained from the augmented model that of Klimanek and Bialecki [17]. In both of the above plots, the tower height is normalized and the rain (rz), fill (fi) and spray (sp) zones are as indicated. The arrows indicate the direction of flow

TABLE 4.4: Geometrical parameters corresponding to the data from the field test described in sub-section 4.1.3.

Tower parameters	
Rain zone height, H_{rz} (m)	4.26
Fill zone height, H_{fi} (m)	1.83
Spray zone height, H_{sp} (m)	0.76
Tower breadth, B_{ct} (m)	14.63
Tower width, W_{ct} (m)	14.63
Number of cells, n	10

4.2 Validation of hybrid cooling tower

The wet-dry augmented model is compared with an example solved by Kröger [4], which uses Merkel's method in the wet section and the e-NTU method in the dry section. The

TABLE 4.5: Comparison of the results obtained using the augmented model vs. analogue field measurements

	m_w (kg/s)	m_a (kg/s)	p_{atm} (Pa)	T_{ai} (K)	T_{wbai} (K)	T_{wi} (K)	T_{wo}^{field} (K)	T_{wo}^{aug} (K)	Absolute error (K)
Test 1 (10:20)	9774.7	5533.8	84,185.0	302.47	290.63	308.61	298.80	298.30	0.50
Test 2 (13:00)	9774.7	5598.3	84,862.9	297.35	289.73	308.18	298.35	297.84	0.51
Test 3 (15:15)	9774.7	5563.4	84,185.0	301.09	290.08	308.45	298.62	298.03	0.59

induced draft hybrid cooling tower is supposed to be fitted with an expanded metal fill and a heat exchanger consisting of four rows of extended bi-metallic finned tubes. The Merkel number for the fill is given by

$$\mathrm{Me}_{fi} = 0.2692\, G_w^{-0.094}\, G_a^{0.6023}\, H_{fi} \tag{4.2}$$

Input variables for the wet and dry sections are given in Table 4.6 and 4.7 respectively. Table 4.8 presents the results obtained from the wet-dry augmented model and from Kröger example [4]. The small discrepancy in the result can again be attributed to the simplifying assumption of the Merkel method. Figure 4.3A and 4.3B respectively show the variation of temperature and humidity in rain (rz), fill (fi), spray (sp) zones and the heat exchanger (he), obtained by solving the wet-dry augmented model.

TABLE 4.6: Input variables for a circular fin type heat exchanger

Input variables	
Outside diameter of core tube (m)	0.02540
Inside diameter of core tube (m)	0.02160
Transversal tube pitch (m)	0.05800
Longitudinal tube pitch (m)	0.05022
Fin diameter (m)	0.05720
Fin thickness (m)	0.00050
Fin pitch (m)	0.00280
Fin tip thickness (m)	0.00025
Fin root thickness (m)	0.00075
Fin root diameter (m)	0.02760
Height of the finned tube bundle (m)	4.00
Thermal conductivity of core tube (W/mK)	17.00
Thermal conductivity of fin (W/mK)	204.00
Mass flow rate of air through dry section (kg/s)	270.01
Number of heat exchanger bundle	8
Number of tube row	4
Number of tubes per row	50
Number of water passes	2

TABLE 4.7: Input variables for the hybrid cooling tower

Input variables	
Type of tower	Rectangular
Breadth of the tower B_{ct} (m)	12.0
Width of the tower W_{ct} (m)	15.0
Air inlet temperature T_{ai} (K)	288.6
Wet bulb temperature of the inlet air T_{wbai} (K)	284.2
Ambient pressure P_{ai} (Pa)	84,100
Water inlet temperature T_{wi} (K)	313.1
Mass flow rate of water m_w (kg/s)	450.0
Mass flow rate of air through wet section m_a^{wet} (kg/s)	482.3
Height of the rain zone H_{rz} (m)	3.5
Height of the fill zone H_{fi} (m)	1.8
Height of the spray zone H_{sp} (m)	0.3

TABLE 4.8: Comparison of the hybrid tower results obtained from wet-dry augmented model with the example of Kröger [4]

Output variables	**Kröger's example [4]**	**Wet-dry augmented model**	**Absolute error**
T_{wo}^{dry} (K)	310.61	310.63	0.02
T_{ao}^{dry} (K)	305.90	305.86	0.04
T_{wo} (K)	296.01	295.61	0.40
T_{ao} (K)	301.55	301.97	-0.42
ω_{ao} (kg/kg)	0.0197	0.0198	-0.0001
ω_{ao}^{wet} (kg/kg)	0.0261	0.0264	-0.0003

4.3 Parametric study of wet cooling tower for different ambient conditions

Having validated the augmented model of section 2.1 in sub-section 4.1.2, we now proceed to assess the predictive capabilities of this model when used in conjunction with the atmospheric dispersion model of Chapter 3. Model predictions are studied for various ambient conditions ranging from hot/dry to cold/wet. The analysis is performed for a tower with dimensions prescribed in Table 4.4. We consider an equal mass flow rate of air and water, i.e. $m_a = m_w = 9774.72\,\text{kg/s}$. The temperature of the inlet water is $T_{wi} = 308.5\,\text{K}$, and atmospheric pressure is $p_{atm} = 84{,}185$ Pa.

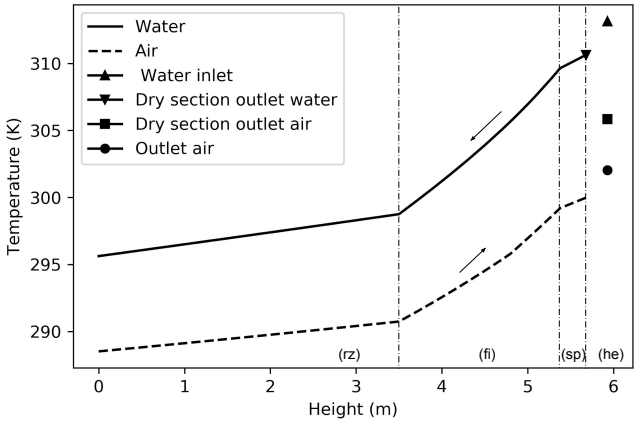

A Distribution of water and air temperature

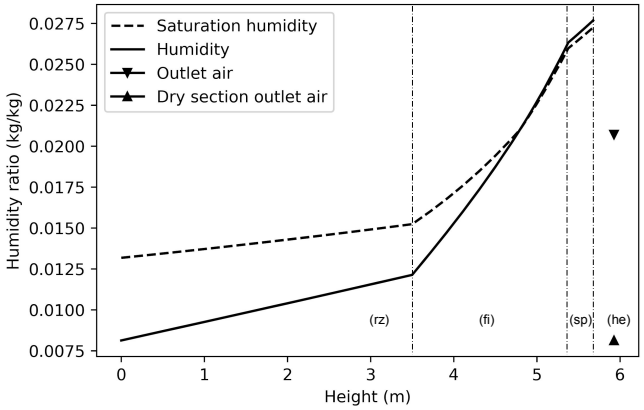

B Distribution of humidity and saturation humidity ratio

FIGURE 4.3: Model output of temperature and humidity obtained from the wet-dry augmented model. In both of the above plots, the tower height is normalized and the rain (rz), fill (fi), spray (sp) and heat exchanger (he) zones are as indicated. The arrows indicate the direction of flow

4.3.1 Hot and humid conditions

For this case, the ambient dry and wet bulb temperatures are chosen to be $T_{ai} = 306.0\,\mathrm{K}$ and $T_{wbai} = 302.6\,\mathrm{K}$ (RH = 78%), respectively, so that the air leaves the tower in a saturated state. The total heat rejected is 231.46 MW, including 229.22 MW and 2.24 MW in the form of latent and sensible heat. The total mass of water evaporated from the tower is 89.4 kg/s. The variation of the temperature and of the relative humidity along height of the cooling tower are respectively presented in Figures 4.4A and 4.4B. Figure 4.4A shows that, until a height of 5.0 m, the air is cooling down instead of warming up. Throughout the entire rain zone and for some part of the fill zone, the sensible heat transfer is from air to water, this due to the large value selected for T_{ai}. As a further manifestation of this fact, Figure 4.4E shows that the ratio of the latent heat transfer to the total heat transfer is greater than (albeit not much greater than) unity. Notwithstanding the large ambient air temperature, the water temperature drops through the rain zone, this as a consequence of evaporative cooling. Meanwhile, Figures

4.4C and 4.4D respectively show the proportion of heat rejected and the mass of water evaporated in the different zones. Figure 4.4F shows the variation of the plume relative humidity with height. The maximum relative humidity of 100% occurs at the plume source. As the plume ascends, its relative humidity decreases due to the entrainment of (comparatively dry) ambient air. Figure 4.4G shows that the quality of air leaving the cooling tower is below saturation curve, as a result, we do not anticipate a visible plume of any significant length in this case.

4.3.2 Hot and dry conditions

Analogue results pertaining to hot and dry conditions with $T_{ai} = 306\,\mathrm{K}$ and $T_{wbai} = 288.81\,\mathrm{K}$ (RH = 17%) are shown in Figure 4.5. The total heat rejected by the cooling tower is 639.44 MW, which includes 664.31 MW (latent) and -24.86 MW (sensible). The total mass of water evaporated in the cooling tower is 260.2 kg/s, almost three times as large as the value reported in sub-section 4.3.1. The variation of the temperature and the relative humidity along the height of the cooling tower are respectively presented in Figures 4.5A and 4.5B. The proportion of the heat rejected and the mass of water evaporated in the different cooling tower zones are respectively presented in Figures 4.5C and 4.5D. Figure 4.5E indicates the ratio of latent heat transfer to total heat transfer (Q_l) where the horizontal line indicates the average value of Q_l/Q_T for the cooling tower as a whole. Figures 4.5F and 4.5G shows the vertical variation of the plume relative humidity. The maximum relative humidity of 98% occurs at the source; for still larger elevations, the plume relative humidity falls owing to the entrainment of ambient air.

4.3.3 Cold and dry conditions

Analogue results pertaining to cold and dry conditions with $T_{ai} = 283.15\,\mathrm{K}$ and $T_{wbai} = 274.7\,\mathrm{K}$ (RH = 17%) are shown in Figure 4.6. The total heat rejected by the cooling tower is 886.77 MW, including 720.34 MW (latent) and 166.43 MW (sensible). The total mass of water evaporated is 282.65 kg/s, more even than is predicted in sub-section 4.3.2. The air, being cold and dry, has a greater capacity to accept latent and sensible heat from the hot water. As such, the air temperature is a monotone increasing function of height. With this steady increase in temperature, the relative humidity also steadily increases, which results in more evaporation overall. As a consequence, air leaves the tower in a super-saturated state as shown in Figure 4.6B. As the direction of latent and sensible heat transfer is the same in all zones, the ratio of latent to total

heat rejected remains below unity–see Figure 4.6E. As shown in Figures 4.6F and 4.6G the plume is visible for roughly 18 m above the top of the cooling tower.

4.3.4 Cold and humid conditions

Analogue results pertaining to cold and humid conditions with $T_{ai} = 283.15\,\mathrm{K}$ and $T_{wbai} = 281.15\,\mathrm{K}$ (RH = 78%) are shown in Figure 4.7. The total heat rejected by the cooling tower is 783.47 MW, including 617.28 MW (latent) and 166.18 MW (sensible). The total mass of water evaporated is 241.9 kg/s. The proportion of heat rejected and the mass of water evaporated in the different cooling tower zones is presented in Figures 4.7C and 4.7D. As in sub-section 4.3.3, the water temperature is always greater than the air temperature resulting in sensible heat transfer from the water to the air. The total sensible heat rejected is almost identical to that from sub-section 4.3.3. On the other hand, there is a 14.3% reduction in the total latent heat rejected. This is due to the fact that the air becomes saturated at the very beginning of the fill zone. Consistent with sub-section 4.3.3, Figure 4.7E shows that $L/Q < 1$. Owing to the cold and humid environmental conditions, we anticipate the longest visible plume of any of the cases explored thus far. Figures 4.7F and 4.7G confirms that this are the case, i.e. it predicts a visible plume have a length of more than 90 m.

4.3.5 Discussion

The augmented model is tested subject to edge-case ambient conditions to evaluate the degree of heat and mass transfer associated with environmental conditions classified as hot and humid, hot and dry, cold and dry, and cold and humid. A summary of results is presented in Table 4.9. When the ambient air is cold, the temperature difference with the inflowing water is larger and sensible heat transfer plays a more significant role, thus maximizing the range i.e. the difference between the inlet and outlet water temperatures. On the other hand, when the ambient air is hot, a small or even negative sensible heat transfer may result. Due to the higher ambient temperature, air has a higher capacity for accommodating water vapor, which enhances the latent heat transfer such that the water temperature can fall below the local air temperature. Temperature reversals of this kind occur inside the fill in Figures 4.4A and 4.5A. Such insights (derived as they are for the case of hot summertime operation), speak to the predictive benefits afforded by the augmented model. By contrast, if all cooling tower zones are lumped into one (with a corresponding average Merkel number), the location

at which the air and water temperatures become equal cannot be ascertained. A similar uncertainty arises even for more pedestrian questions e.g. "Where does the air become saturated with water vapor?"

TABLE 4.9: Summary of the results for the four different ambient conditions examined in section 5.

	Range (K)	Q_T (MW)	Q_L (MW)	Q_S (MW)	m_{evp} (kg/s)	H_{plume} (m)
Hot and dry	15.07	639.44	664.31	-24.86	260.2	0
Hot and humid	5.48	231.46	229.22	2.24	89.4	0
Cold and dry	21.21	886.77	720.34	166.43	282.65	17.9
Cold and humid	18.79	783.47	617.28	166.18	241.9	90.09

4.4 Parametric study of hybrid cooling tower for various ambient conditions

Having validated the hybrid model i.e. wet-dry augmented model in sub-section 4.2, we now proceed to assess the predictive capabilities of this model when used in conjunction with the atmospheric dispersion model of Chapter 3. The model predictions are studied for various ambient conditions, such as hot/dry, hot/humid, cold/dry, and cold/humid. The analysis is performed for a hybrid tower whose dimensions are prescribed in Tables 4.6 and 4.7. The temperature of the inlet water is $T_{wi} = 313.1\,\mathrm{K}$ and atmospheric pressure is $p_{atm} = 84{,}100\,\mathrm{Pa}$.

4.4.1 Hot and humid conditions

The dry and wet bulb temperatures are chosen to be $T_{ai} = 306.0\,\mathrm{K}$ and $T_{wbai} = 302.6\,\mathrm{K}$ (RH = 78%), respectively. In this case, the total heat rejected in the hybrid cooling tower is 14.24 MW, which includes 13.63 MW and 0.61 MW from wet and dry sections, respectively. The total mass of water evaporated from the tower is 5.16 kg/s, and the presence of a dry section conserves 0.35 kg/s of water. The variation of temperature and relative humidity along the hybrid cooling tower are presented in Figures 4.8A and 4.8B. The dry section cools the hot water by a considerable amount (0.6 K) and the rest of the cooling of 7.17 K happens in the wet section–see Figure 4.8A. The relative humidity of air leaving the wet section is around 95%, however, due to the influx of dry air from the dry section the air exiting the tower has a relative humidity of only

81% – see Figure 4.8B. Consequently, no visible plume is anticipated as confirmed by Figure 4.8C.

4.4.2 Hot and dry conditions

Analogue results pertaining to hot and dry conditions with T_{ai} = 306 K and T_{wbai} = 288.81 K (RH = 17%) are shown in the Figures 4.9A, 4.9B and 4.9C. The total heat rejected in the tower is 26.66 MW, which includes 26.05 MW and 0.61 MW from the wet and dry sections, respectively. The total mass of water evaporated in the cooling tower is 10.62 kg/s. The heat rejected in the wet section is almost twice that from sub-section 4.4.1, however, the heat rejected in the dry section remains the same because the dry-bulb temperature is unchanged. The variation of temperature and relative humidity along the hybrid cooling tower are presented in Figures 4.9A and 4.9B. Similar to the hot and humid conditions, the air leaving the cooling tower is below saturation, therefore, there is no visible plume as shown in the Figure 4.9C.

4.4.3 Cold and dry conditions

Analogue results pertaining to cold and dry conditions with T_{ai}= 283.15 K and T_{wbai}= 274.7 K (RH = 17%) are shown in Figures 4.10A, 4.10B and 4.10C. The total heat rejected by the tower is 33.35 MW, which includes 2.51 MW and 30.84 MW from wet and dry sections, respectively. Because the air is cold, it has a greater capacity to accept sensible heat from the hot water. As a consequence, the heat rejected in the dry section is four times larger than the value reported in sub-section 4.4.2. The dry section cools the hot water by 2.68 K and the rest of the cooling of 19.1 K happens in wet section–see Figure 4.10A. Figure 4.10A indicates that the air temperature is a monotone increasing function of height. With this steady increase in air temperature, the relative humidity also increases, which results in more water evaporation. The total amount of water evaporated in the cooling tower is 10.13 kg/s, almost close to the value predicted in sub-section 4.4.2. As a result of the heat rejected in the dry section, 1.2 kg/s of water are conserved. Figure 4.10B indicates that the air becomes saturated at around 4.7 m and leaves the wet section as super-saturated air. The hot and dry air from the dry section dilutes the air from the super-saturation to sub-saturation i.e. from a relative humidity ratio of 0.0241 kg/kg to 0.01670 kg/kg. Figure 4.10C indicates that a visible plume of height 10.2 m is abated by using the hybrid tower.

4.4.4 Cold and humid conditions

Analogue results pertaining to cold and humid conditions with T_{ai} =283.15 K and T_{wbai} = 281.15 K (RH = 78%) are shown in Figure 4.11A, 4.11B and 4.11C. The total heat rejected in the hybrid tower is 29.78 MW, which includes 2.51 MW and 27.72 MW from dry and wet sections, respectively. The total heat rejected from dry section is equal to that from sub-section 4.4.3; as noted above, the performance of a dry section is a function of the dry-bulb temperature but not the wet-bulb temperature. The total cooling realized by the tower is 20.10 K. The air from the wet cooling tower gets saturated around 4.5 m, and becomes super-saturated at the exit of the wet section. Hot air from the dry section reduces the relative humidity of the air from the super-saturated to the under-saturated region, i.e. from a relative humidity ratio of 0.0276 kg/kg to 0.0206 kg/kg, as shown in Figure 4.11B. The comparison of visible plume height for wet vs. hybrid cooling towers is presented in Figure 4.11C.

4.4.5 Discussion

A summary of key results from the preceding four sub-sections is presented in Table 4.10.

TABLE 4.10: Summary of results for the four different environmental conditions examined in section 4.4

	Range (K)	Q_T (MW)	Q_{dry} (MW)	Q_{wet} (MW)	m_{evap} (kg/s)	H_{plume} (m)
Hot and dry	14.53	26.66	0.61	26.05	10.62	0
Hot and humid	7.17	14.24	0.61	13.63	5.16	0
Cold and dry	21.70	33.35	2.51	30.84	10.13	0
Cold and humid	20.10	29.78	2.51	27.72	8.92	0

When the ambient air is cold, the temperature difference with the inflowing water is large and sensible heat transfer plays a more significant role, thus maximizing the performance of the dry section. Correspondingly, there can exist a large difference of temperatures between the water sent to the tower vs. that sent to the wet section of the tower. Due to the lower ambient temperature, air has a lesser capacity for accommodating water vapor. Although some sensible heating of this cold air occurs, the air stream nonetheless leaves the wet section in a super-saturated state. The heated air stream from the dry section mixes and dilutes this wet air stream to avoid formation of a visible plume as shown in Figures 4.10B and 4.11B. On the other hand, when the ambient air is hot, the thermal performance of the dry section plummets, as shown in Figures 4.9A and 4.8A. Due to the higher ambient temperature, air has a higher capacity for accommodating water vapor, therefore, the humidity of the air leaving

the wet section may fall below saturation as shown in Figures 4.9B and 4.9B. As a consequence, there is a diminished likelihood of a visible plume. Of course, the fraction of air directed to the wet vs. dry sections of real hybrid towers can be modified in real time using louvers, whether of the manual or computer-controlled variety. Making such adjustments (e.g. for the purpose of directing more air to the wet section in summer and more air to the dry section in winter) provides industries with an opportunity to maximize thermal performance throughout the year.

4.5 Parametric study for different operating parameters

4.5.1 Parametric study of a hybrid cooling tower for different L/G ratios

The purpose of this sub-section is to study how plume visibility, range, and water evaporation changes as the flow rates of air entering the wet and dry sections are varied. In this examination, the mass flow rate of water, L, has been kept constant and equal to 1000 kg/s, while the flow rate of air entering the tower is varied. Visible plumes are more predominant when the ambient conditions are cold and humid [6, 7]. Wishing to focus on cases where visible plume formation is, by turns, likely or possible, we shall here consider $T_{ai} = 263.15\,\mathrm{K}$ and $T_{ai} = 278.15\,\mathrm{K}$. In either case, the relative humidity measures 77%. Tables 4.6 and 4.7 show the geometrical parameters of the hybrid cooling tower of interest. Model output is summarized in figures 4.12 and 4.13, which show for $T_{ai} = 263.15\,\mathrm{K}$ and $T_{ai} = 278.15\,\mathrm{K}$, respectively, the variation of visible plume height, range, and water evaporation for different L/G ratios and the mass flow rate of air entering the wet and dry sections.

As the total mass flow rate of air increases (i.e. as L/G decreases), there is a more robust transfer of heat and mass within the cooling tower. In turn, this yields a larger range and higher rates of water evaporation, as shown in Figures 4.12B,4.12C and 4.13B,4.13C. Moreover, and because the heat and mass absorbed from the water is distributed over a greater volume of air, one observes a smaller increase of air temperature and relative humidity at the tower exit [9]. As a consequence, the visible plume height decreases with increasing mass flow rate of air, as shown in Figures 4.12A, 4.13A. The visible plume height (and overall rate of water loss by evaporation) can also be decreased by increasing the proportion of air directed to the dry section, as indicated in Figures 4.12C, 4.13C and 4.12A,4.13A. On the other hand, increasing the proportion of air directed to the dry section decreases the cooling range of a tower–see Figures 4.12B

and 4.13B. This is because the wet section provides more efficient cooling than does the dry section.

4.5.2 Parametric study of a hybrid cooling tower for different fill types

In this sub-section a comparative study is performed to characterize the performance of different film-type fills, i.e. those produced by Brentwood Industries, Inc. We choose to examine fills of different flute configuration such as cross-fluted (CF1200AT), vertical-fluted (VF3800), and offset-vertical (OF21MA and OF20SB). Here, and although we fix $L/G = 1$ and specify a fill height of 1 m, we allow the proportion of air flowing to the dry vs. wet sections to vary. The simulations are carried out for cold and cool ambient conditions i.e. $T_{ai} = 278.15\,\mathrm{K}$ and $T_{ai} = 288.15\,\mathrm{K}$, respectively. In either case the relative humidity is maintained at 77%. Geometrical parameters of the hybrid tower are again given in Tables 4.6 and 4.7.

In a cross-fluted fill configuration (CF1200AT) water is distributed by splitting the water stream as it descends through the fill. Cross-fluted fill thereby offers higher thermal performance by maximizing the contact surface and time. This generic conclusion is supported by our numerical results. For example, Figures 4.14B and 4.15B show that a cross-fluted fill offers superior thermal performance vs. vertical-fluted and offset-vertical fills. In a vertical-fluted fill (VF3800), water descends through a vertical channel. These types of fill offer inferior thermal performance in comparison with cross-fluted fills. On the other hand, vertical-fluted fills can be operated at higher water flow rates, and are therefore less prone to fouling. Finally, offset-vertical fills (OF21MA and OF20SB) are a combination of a vertical-fluted and cross-fluted fill. This combination provides an anti-fouling environment and thermal performance that is superior to a strictly vertical-fluted fill–see Figures 4.15B and 4.14B. Also included in these figures is a Brentwood Industries fill labeled as AFVF19, which is "designed with engineered micro-structure for high thermal performance". The fill in question fill offers better thermal performance in comparison with its counterparts considered in this study. As expected, with the increase in thermal performance of the fill, the heat and mass transfer in the fill also increases. As a consequence, the water evaporation, cooling range, and the length of visible plume height also increase, as shown in Figure 4.15A, 4.14A, 4.15C, and 4.14C.

4.5.3 Parametric study of a hybrid cooling tower for different fill heights

In this sub-section, simulations are performed to study the influence of fill height on the thermal performance of a hybrid cooling tower and on the visible plume length. In this examination, we vary the fill height and the fraction of air directed towards the dry section. Consistent with our previous discussion, $L/G = 1$ and the geometric parameters that define the cooling tower are prescribed in Tables 4.6 and 4.7. We choose to consider an offset-vertical type fill (OF21MA) as these kinds of fill offer generally good thermal performance and anti-fouling behavior. Simulations are preformed for cold and cool ambient temperatures of $T_{ai} = 278.15\,\mathrm{K}$ and $T_{ai} = 288.15\,\mathrm{K}$, where, in either case, the relative humidity measures 77%. The variation of cooling range, water evaporation, and visible plume height for $T_{ai} = 278.15\,\mathrm{K}$ and $T_{ai} = 288.15\,\mathrm{K}$ are presented in Figures 4.16 and 4.17, respectively.

As the fill height increases, there is a robust increase in the heat and mass transfer within the wet section. By extension, this yields larger cooling range and higher amount of water evaporation, as shown, respectively, in Figures 4.16B, 4.17A and 4.16C, 4.17A. Increasing the fill height maximizes the contact surface and contact time between air and water, thus promoting more heat and mass transfer. Moreover, the temperature and relative humidity of air leaving the fill also increases with the increase in fill height. As a result, the length of the visible plume also increases, as shown in Figures 4.16A and 4.17A. However, with the increase in fill height the pressure drop across the fill also increases [22, 47], resulting in more fan power, by extension, increased operational cost. As discussed in sub-section 4.5.1, the water evaporation and visible plume height can be curtailed by directing more air towards the dry section.

4.5.4 Parametric study of a hybrid cooling tower for different number of tubes per row

In this sub-section, we examine the performance of a hybrid cooling tower for different numbers of tubes per row in the dry section and the amount of air directed towards this dry section. The study was performed for cold and cool ambient conditions at a relative humidity of 77%. We consider film type fill (OF21MA) of height 1 m. Other geometrical parameters for the wet and dry sections are provided in Tables 4.6 and 4.7. The variation of visible plume height, mass of water evaporated, and range are presented in Figures 4.18A, 4.19A, 4.18B, 4.19B, and 4.18C, 4.19C respectively. As the number of tubes per row in the dry section increases, the amount of heat rejected in the dry section also increases. This increases the outlet air temperature and cooling

range in the dry section. As a result, the air leaving the cooling tower is pushed from a super-saturation region to a sub-saturation region. The visible plume length decreases, as shown in the Figure 4.18A. Furthermore, the amount of water evaporated decreases with an increase in number of tubes per row.

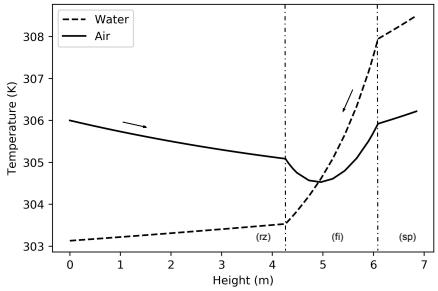

A Variation of water and air temperatures in the cooling tower

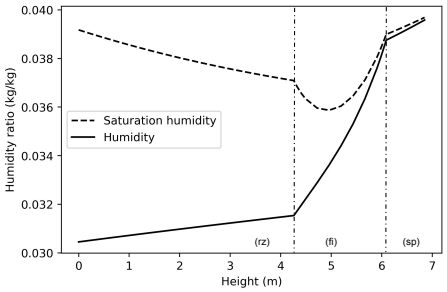

B Variation of humidity and saturation humidity in the cooling tower

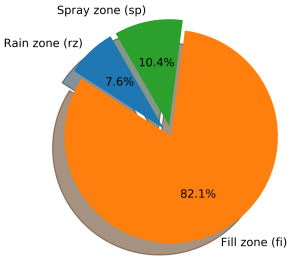

C Proportion of heat rejected by cooling tower zone

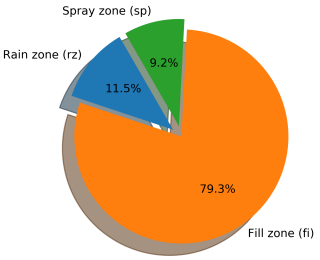

D Water evaporated by cooling tower zone

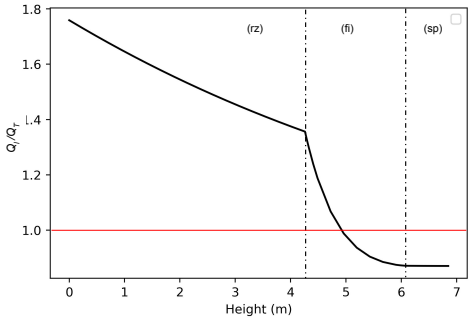

E Ratio of the rejected latent heat, Q_l, to the total rejected heat, Q_l. The horizontal line indicates the average value across the tower

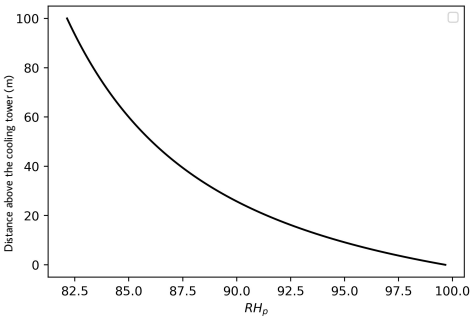

F Variation of the plume relative humidity with height

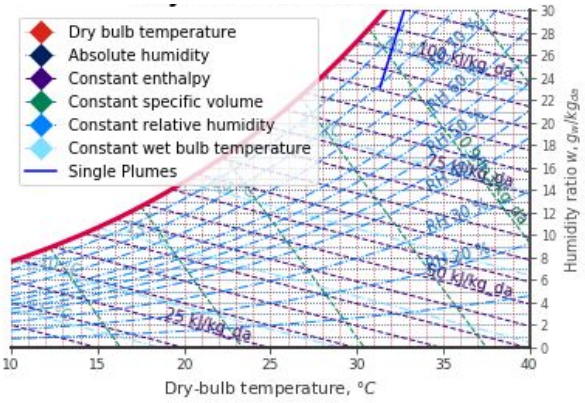

G Psychrometric chart representing the evolution of the plume

FIGURE 4.4: Hot and humid conditions corresponding to the example of subsection 4.3.1

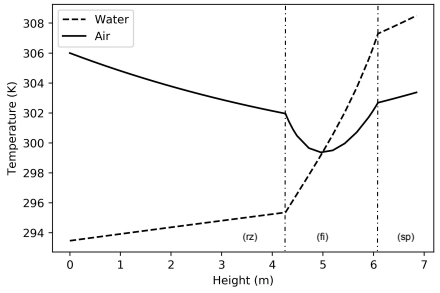

A Variation of water and air temperatures in the cooling tower

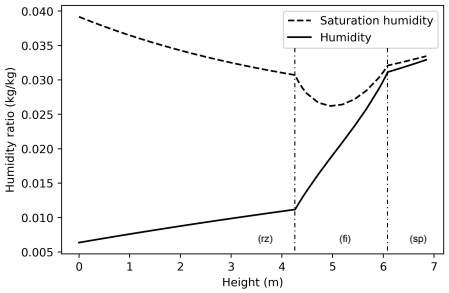

B Variation of humidity and saturation humidity in the cooling tower

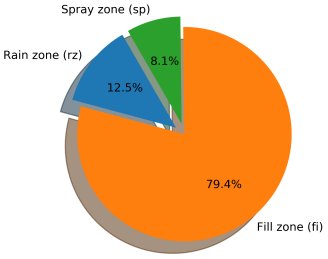

C Proportion of heat rejected by cooling tower zone

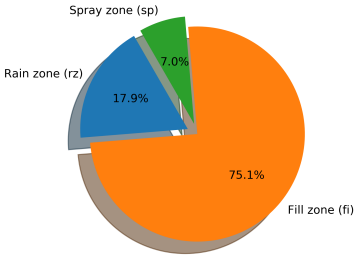

D Water evaporated by cooling tower zone

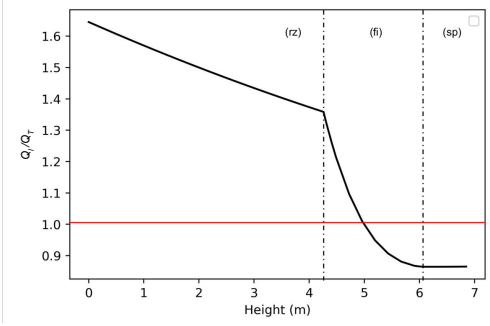

E Ratio of the latent heat, Q_l, to the total rejected heat, Q_T. The horizontal line indicates the average value across the tower

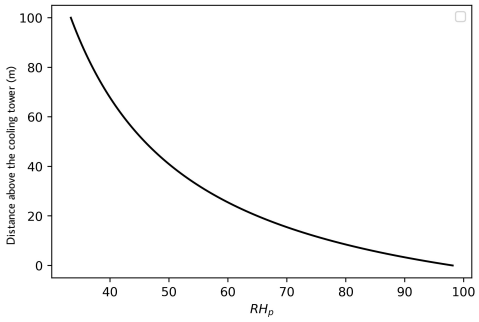

F Variation of the plume relative humidity with height.

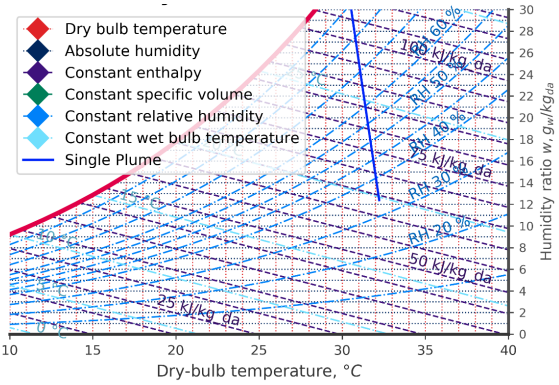

G Psychrometric chart representing the evolution of the plume

FIGURE 4.5: Hot and dry conditions corresponding to the example of sub-section 4.3.2

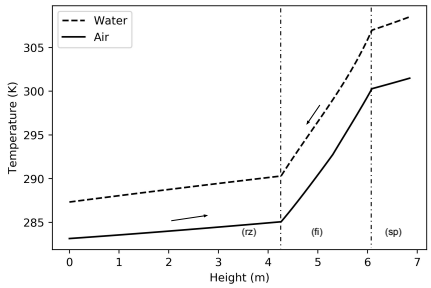

A Variation of water and air temperatures in the cooling tower

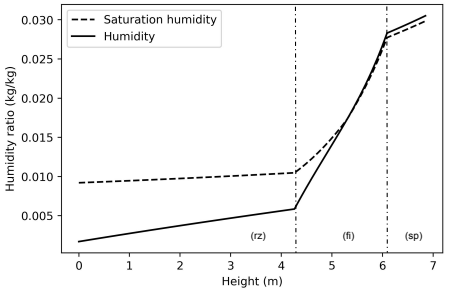

B Variation of humidity and saturation humidity in the cooling tower

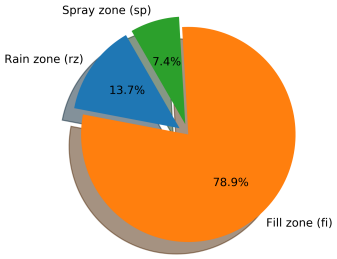

C Proportion of heat rejected by cooling tower zone

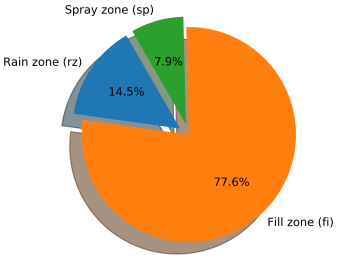

D Water evaporated by cooling tower zone

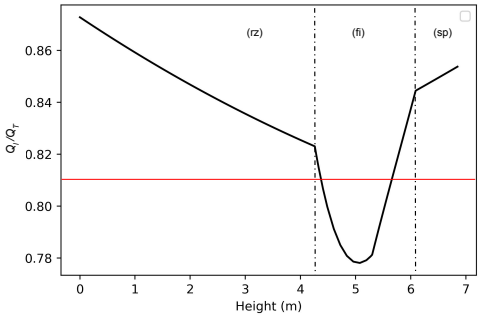

E Ratio of the latent heat, Q_l, to the total rejected heat, Q_T. The horizontal line indicates the average value across the tower

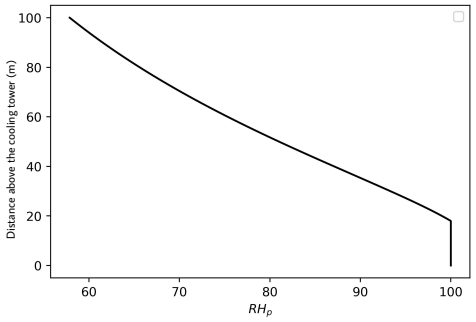

F Variation of the plume relative humidity with height.

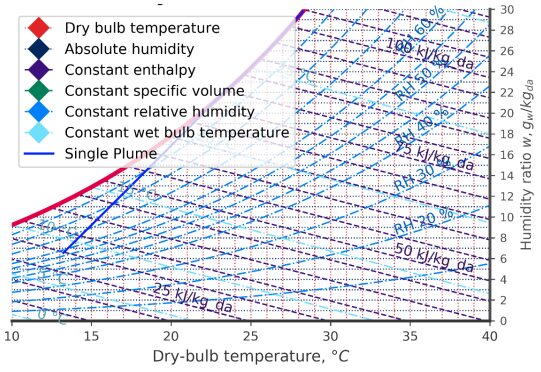

G Psychrometric chart representing the evolution of the plume

FIGURE 4.6: Cold and dry condition corresponding to the example of section 4.3.3

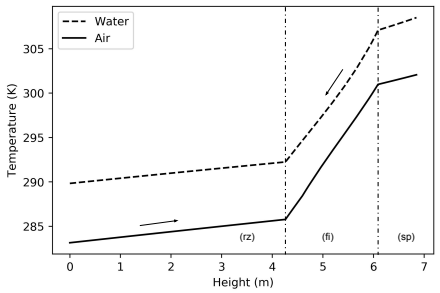

A Variation of water and air temperatures in the cooling tower

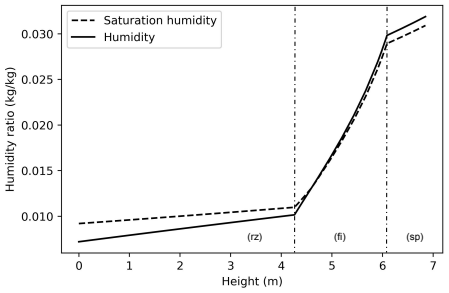

B Variation of humidity and saturation humidity in the cooling tower

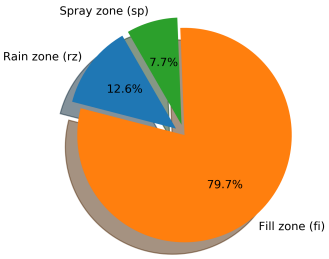

C Proportion of heat rejected by cooling tower zone

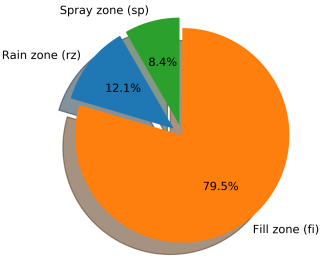

D Water evaporated by cooling tower zone

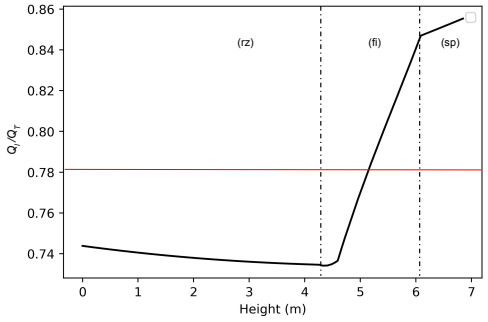

E Ratio of the latent heat, Q_l, to the total rejected heat, Q_T. The horizontal line indicates the average value of Q_l/Q_T for a cooling tower.

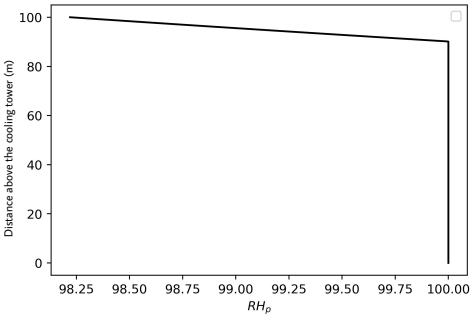

F Variation of the plume relative humidity with height.

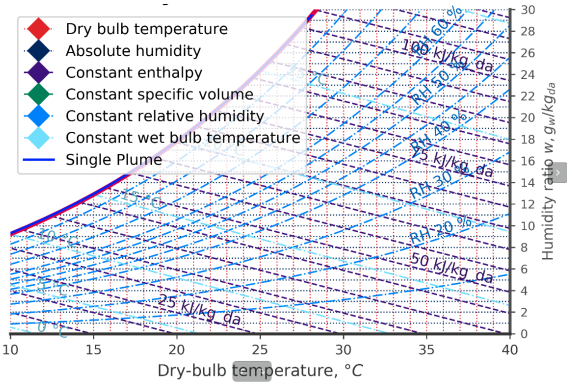

G Psychrometric chart representing the evolution of the plume

FIGURE 4.7: Cold and humid condition corresponding to the example of section 4.3.4

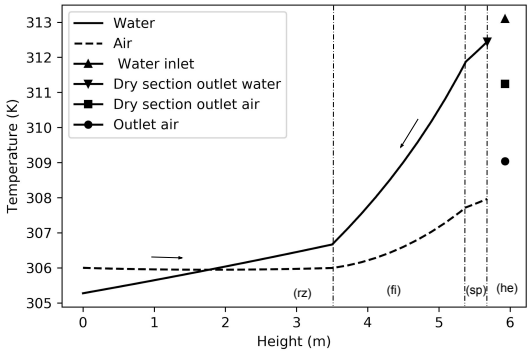

A Variation of water and air temperature in the hybrid cooling tower. In this figure, ▲ and ▼ represent the inlet and outlet water temperatures for the dry section, ■ represents the air temperature at the exit of dry section, and ● represents the air temperature at the exit of the cooling tower

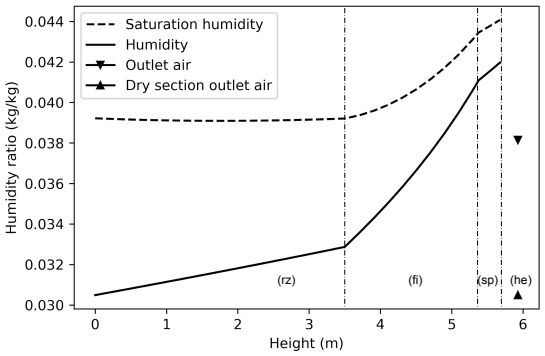

B Variation of humidity and saturation humidity in the hybrid cooling tower. ▲ represents the humidity of air at the exit of the dry section and ▼ represents the humidity of the air at the exit of the cooling tower

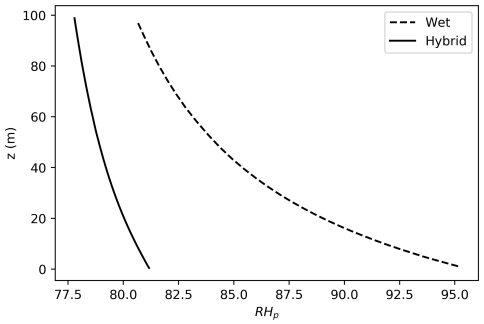

C Variation of the plume relative humidity with vertical distance above the fan shroud. The continuous line represents the evolution of plume for the hybrid cooling tower, and the discontinuous line shows the evolution of the plume in the absence of a dry section

FIGURE 4.8: Hot and humid conditions corresponding to the example of section 4.4.1

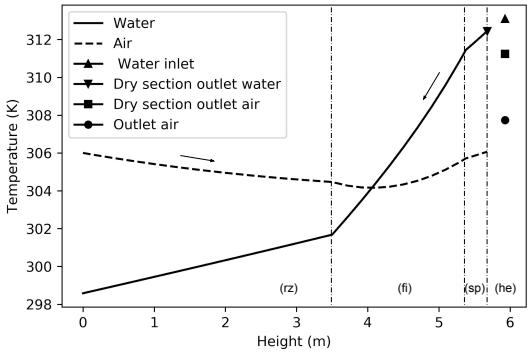

A As in Figure 4.8A but for the example of sub-section 4.4.2

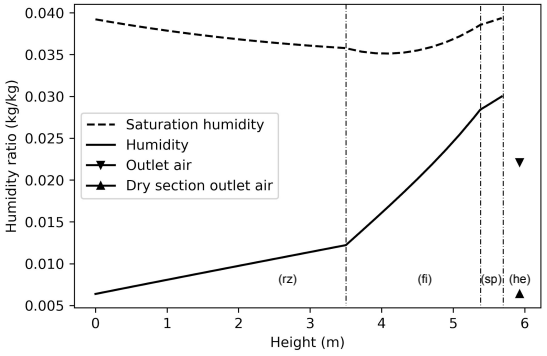

B As in Figure 4.8B but for the example of sub-section 4.4.2

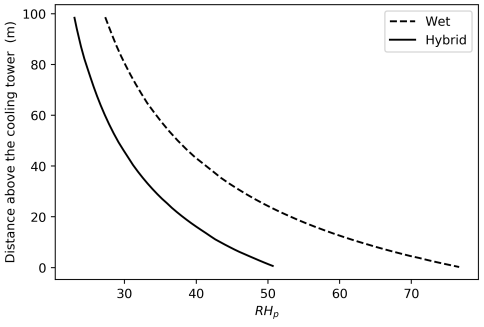

C As in Figure 4.8C but for the example of sub-section 4.4.2

FIGURE 4.9: Hot and dry conditions corresponding to the example of sub-section 4.4.2

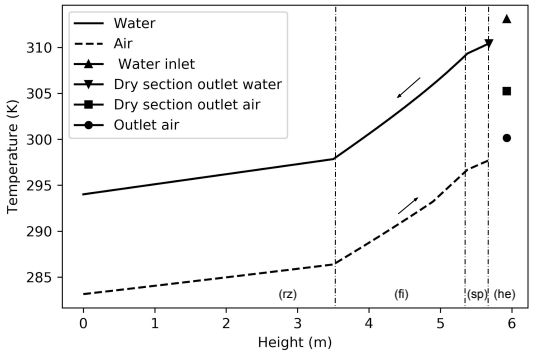

A Variation of water and air temperature in the hybrid cooling tower. In this figure, ▲ and ▼ represents the inlet and outlet water temperatures for the dry section, ■ represents the outlet air temperature at the exit of dry section, ● represents the air temperature at the exit of cooling tower

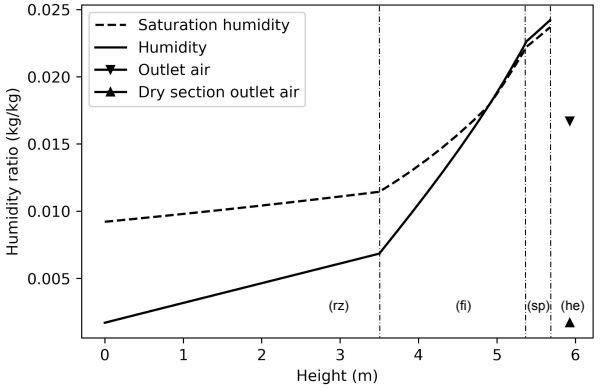

B Variation of humidity and saturation humidity in the hybrid cooling tower. Where ▲ represents the humidity of air at the exit of dry section and ▼ represents the humidity of air at the exit of cooling tower

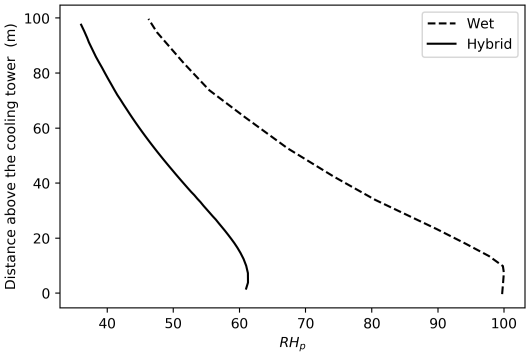

C Variation of relative humidity of the plume along the vertical height. The continuous line represents the evolution of plume for the hybrid cooling tower, and the discontinuous line shows the evolution of plume in the absence of a dry section

FIGURE 4.10: Cold and dry conditions corresponding to the example of sub-section 4.4.3

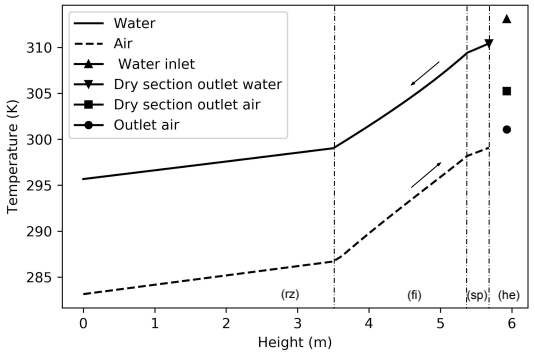

A As in Figure 4.10A but for the example of sub-section 4.3.4

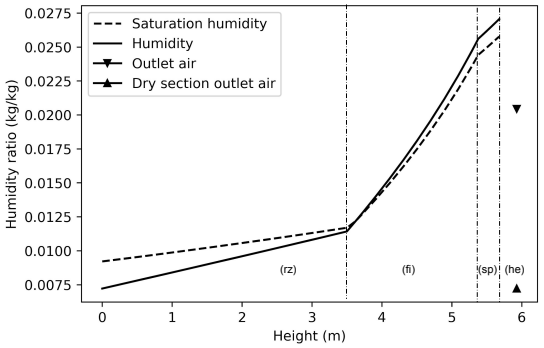

B As in Figure 4.10B but for the example of sub-section 4.3.4

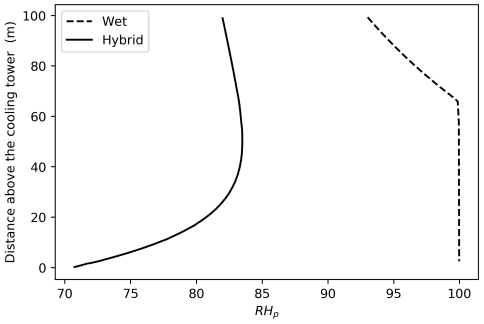

C As in Figure 4.10C but for the example of sub-section 4.3.4

FIGURE 4.11: Cold and humid conditions corresponding to the example of sub-section 4.4.4

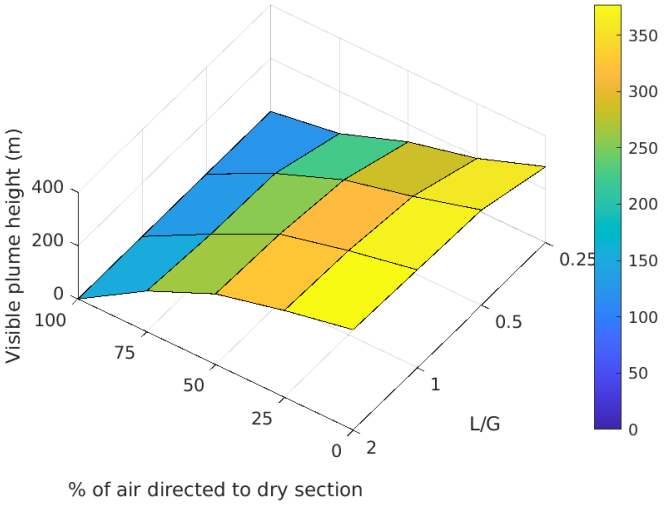

A Variation of the visible plume height as a function of L/G ratio and the proportion of air directed to dry section.

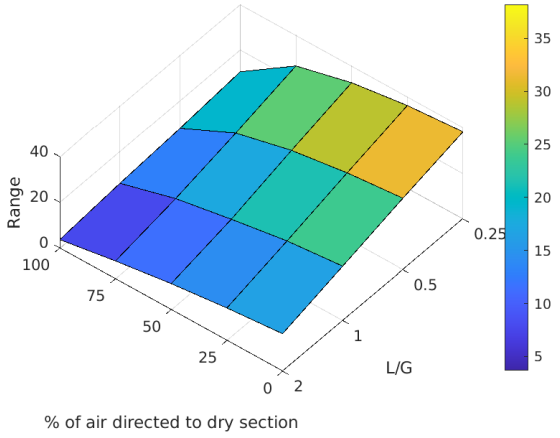

B Variation of the cooling range as a function of L/G ratio and the proportion of air directed to dry section.

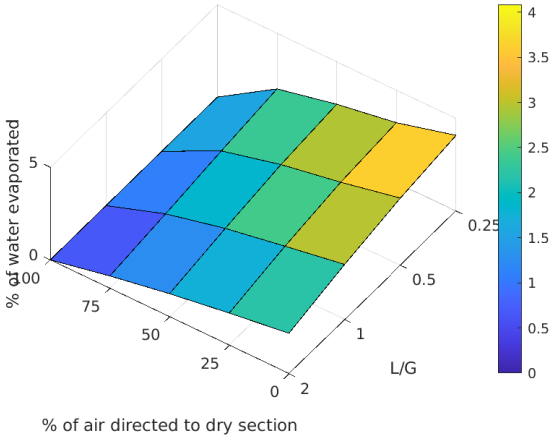

C Variation of the water evaporated as a function of L/G ratio and the proportion of air directed to dry section.

FIGURE 4.12: Performance of a hybrid cooling tower operating at a dry bulb temperature of 263.15 K at 77% relative humidity

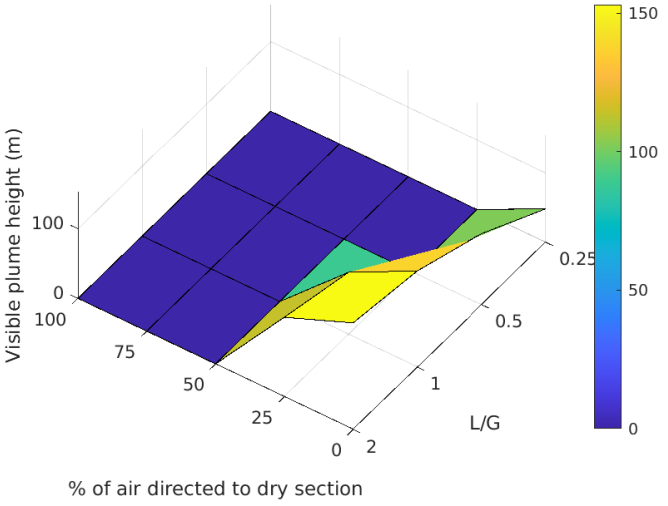

A Variation of the visible plume height as a function of L/G ratio and the proportion of air directed to dry section.

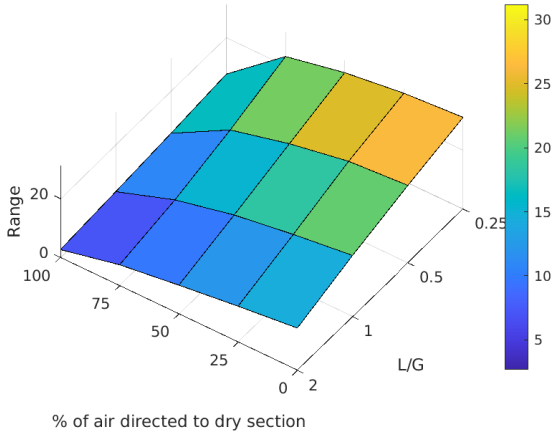

B Variation of the cooling range as a function of L/G ratio and the proportion of air directed to dry section.

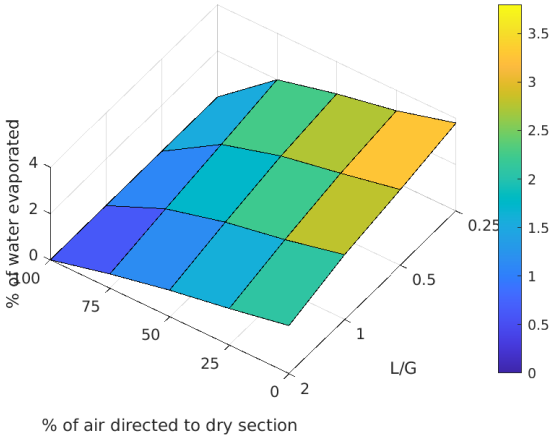

C Variation of the water evaporated as a function of L/G ratio and the proportion of air directed to dry section.

FIGURE 4.13: Performance of a hybrid cooling tower operating at a dry bulb temperature of 278.15 K at 77% relative humidity

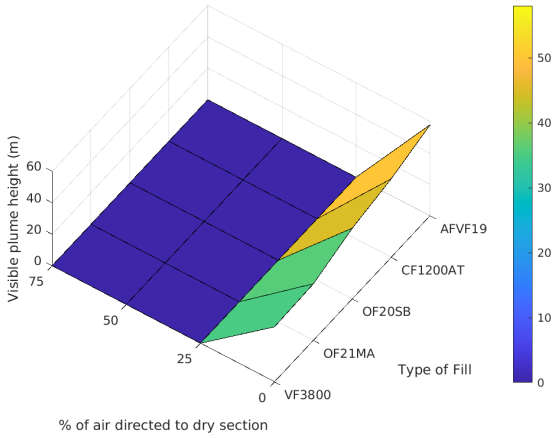

A Variation of the visible plume height for different fill types and as a function of the proportion of air directed to dry section.

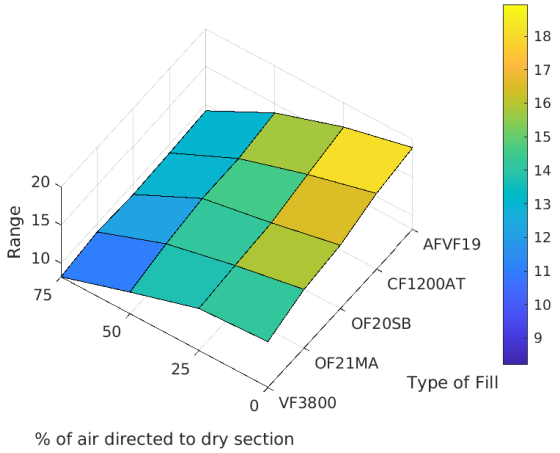

B Variation of the cooling range for different fill types and as a function of the proportion of air directed to dry section.

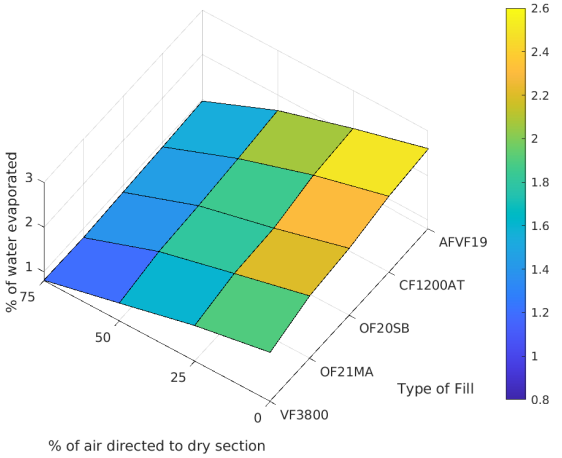

C Variation of the water evaporated for different fill types and as a function of the proportion of air directed to dry section.

FIGURE 4.14: Performance of a hybrid cooling tower operating at a dry bulb temperature of 288.15 K at 77% relative humidity

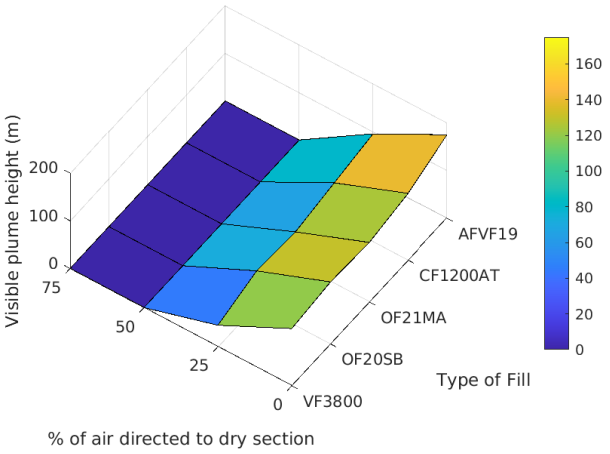

A Variation of the visible plume height for different fill types and the proportion of air directed to dry section.

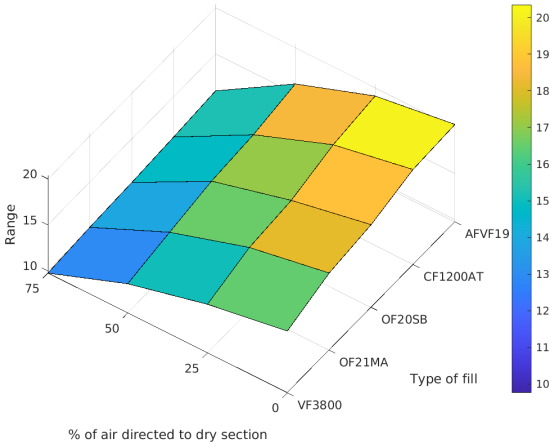

B Variation of the cooling range for different fill types and the proportion of air directed to dry section.

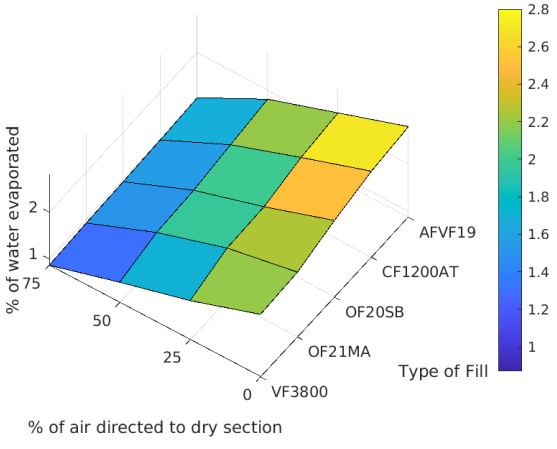

C Variation of the water evaporated for different fill types and the proportion of air directed to dry section.

FIGURE 4.15: Performance of a hybrid cooling tower operating at a dry bulb temperature of 278.15 K at 77% relative humidity

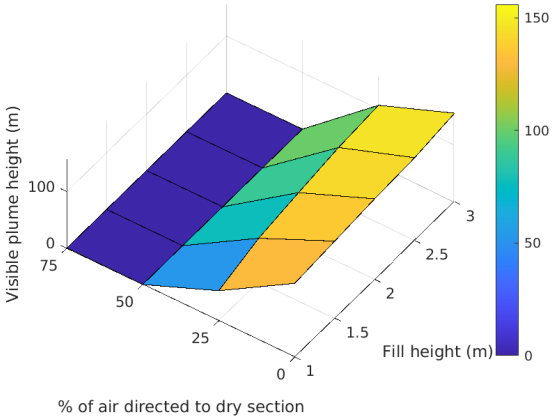

A Variation of the visible plume height as a function of fill height, H_{fi}, and the proportion of air directed to dry section.

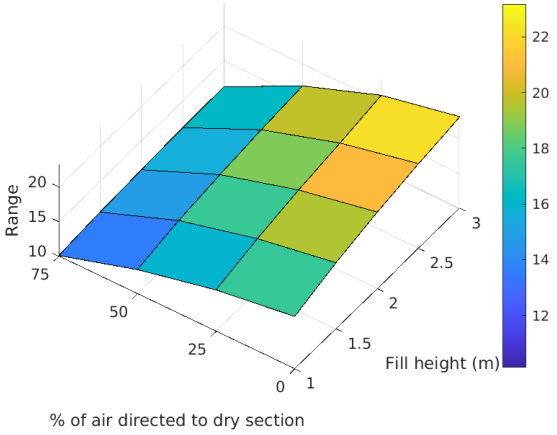

B Variation of the cooling range as a function of fill height, H_{fi}, and the proportion of air directed to dry section.

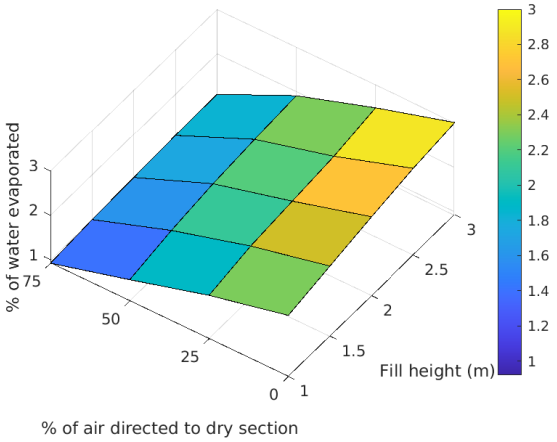

C Variation of the water evaporated as a function of fill height, H_{fi}, and the proportion of air directed to dry section.

FIGURE 4.16: Performance of a hybrid cooling tower operating at a dry bulb temperature of 278.15 K at 77% relative humidity

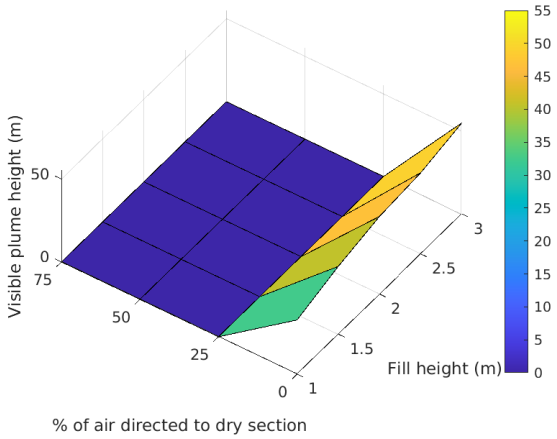

A Variation of the visible plume height as a function of fill height, H_{fi}, and the proportion of air directed to dry section.

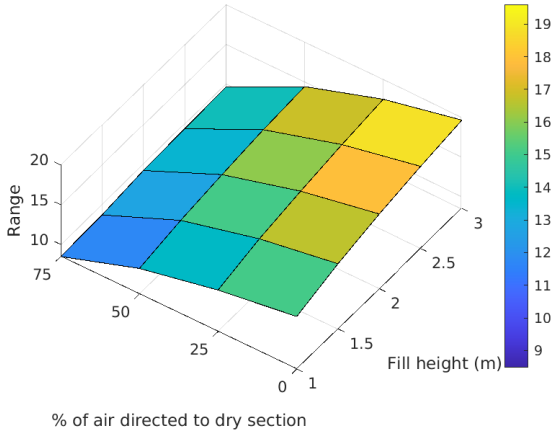

B Variation of the cooling range as a function of fill height, H_{fi}, and the proportion of air directed to dry section.

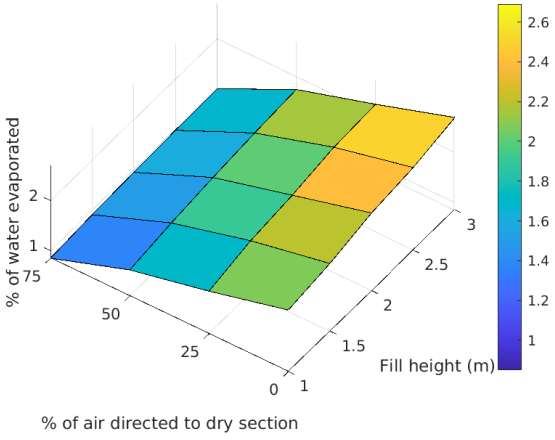

C Variation of the water evaporated as a function of fill height, H_{fi}, and the proportion of air directed to dry section.

FIGURE 4.17: Performance of a hybrid cooling tower operating at a dry bulb temperature of 288.15 K at 77% relative humidity

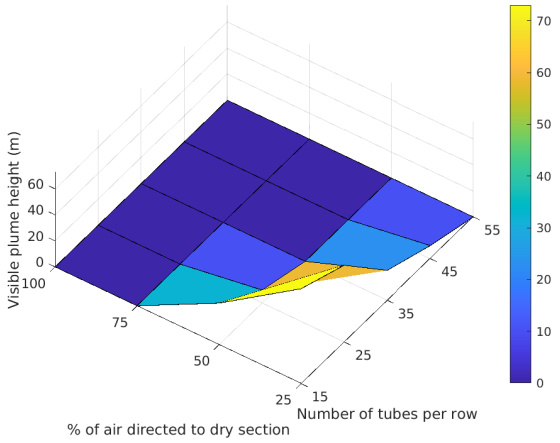

A Variation of the visible plume height for different number of tubes per row and the proportion of air directed to dry section.

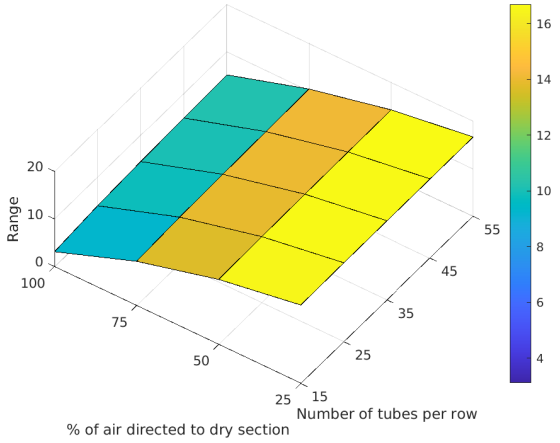

B Variation of the cooling range for different number of tubes per row and the proportion of air directed to dry section.

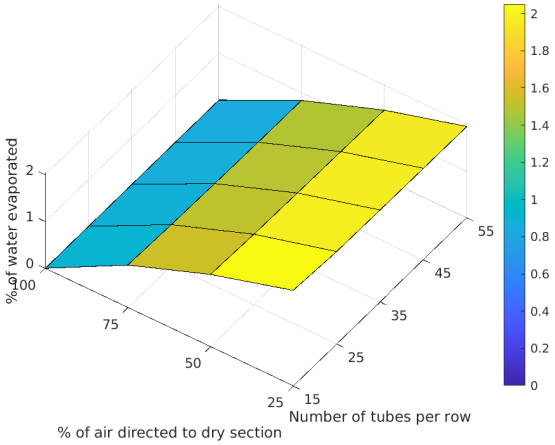

C Variation of the water evaporated for different number of tubes per row and the proportion of air directed to dry section.

FIGURE 4.18: Performance of a hybrid cooling tower operating at a dry bulb temperature of 278.15 K at 77% relative humidity

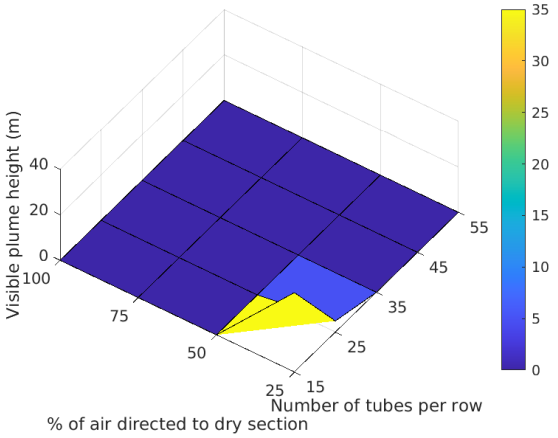

A Variation of the visible plume height for different number of tubes per row and the proportion of air directed to dry section.

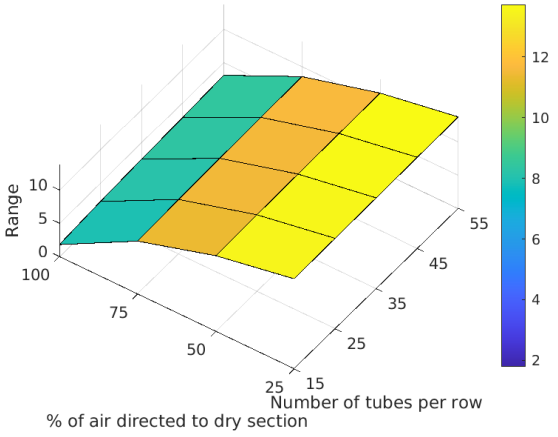

B Variation of the cooling range for different number of tubes per row and the proportion of air directed to dry section.

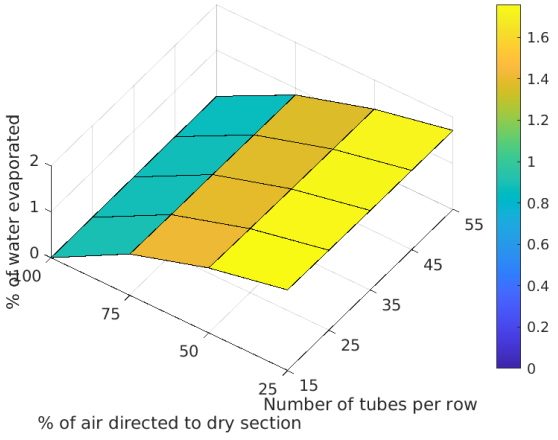

C Variation of the water evaporated for different number of tubes per row and the proportion of air directed to dry section.

FIGURE 4.19: Performance of a hybrid cooling tower operating at a dry bulb temperature of 288.15 K at 77% relative humidity

Chapter 5

Conclusion and Future work

5.1 Conclusion

A steady state mathematical model is developed to predict the thermodynamic performance of a hybrid cooling tower and to forecast the likelihood of a visible plume. The developed model cannot reliably predict the start-up transients process that may arise in a hybrid cooling tower. For example, the initial flow velocity driven by the draft force. To this end, a wet cooling tower model is developed, that describes the heat and mass transfer processes that occur within an induced-draft cooling tower. Although this model is based on the previous study conducted by Klimanek and Bialecki [17], it extends this earlier work in important ways. Most especially, we separately consider the influence of the spray, fill and rain zones, each of which is modelled with reference to its own Merkel number correlation.

In the dry section, which consists of a finned tube heat exchanger and which is located above the wet section, we do not define a Merkel number. Rather, and following standard practice, we implement an e-NTU model so as to predict the rate of heat transfer. The primary function of a dry section is to reduce the humidity of saturated air emanating from the wet section. Depending on the amount of heat dissipated in a dry section, the humidity of air leaving the tower may be substantially reduced, and, as an additional benefit, the rate of water loss may be curtailed. To predict the thermodynamic evolution of the hot, moist air discharged by the tower to the atmosphere and to develop strategies for abating the visible plume, a turbulent plume model based on the conservation of mass, momentum, heat, and moisture is adapted from the work of Wu and Koh [1] and and Li et al. [26]. An attractive feature of Wu and Koh's model is that it considers the merging of plumes emanating from multiple cooling cells. This

model can accommodate the change in overall shape and in the ambient entrainment rate that results from merging. As a result, we anticipate robust predictions for the visible plume height and the likelihood of plume formation.

Wet cooling tower model results are verified with analogue analytical models [35, 46] in sub-sections 4.1.2 and 4.1.1. Figure 4.2 illustrates the difference between a zone-centric model and the lumped analysis of Klimanek and Bialecki [17]. In section 4.1.3, the model is validated against data collected in August 2015 during a performance test conducted by International Cooling Tower, Inc. on a cooling tower installation located in Colorado. Also, the developed wet-dry augmented model is compared with an example problem from Kröger [4]–in sub-section 4.2. Based on these comparisons, the following general conclusions may be drawn: (i) the developed wet cooling tower model makes predictions that are in good agreement with related analytical models and with complementary field data and, (ii) the implemented e-NTU model shows good agreement with the example problem of Kröger's.

Having validated our model with respect to previously published results/collected data, sections 4.3 and 4.4 proceeds to quantify, for different ambient and operating conditions, the amount of heat rejected through latent or sensible effects. Through this analysis, we find from Figures like 4.4C, 4.5C, 4.6C and 4.7C that the combined cooling contribution due to the spray and rain zones is around 18% to 22% of total cooling. These fractions, though modest in comparison to the contribution of the fill zone, are sufficiently large as to merit separate consideration in a robust cooling tower model. Furthermore, from Figures 4.4 and 4.5A we can observe that the rain zone adversely affects cooling performance during hot ambient conditions. From a design point of view, it may therefore be advantageous to limit the rain zone height, an insight that cannot be derived when the disparate tower zones are lumped altogether.

A zone-centric modelling approach has other advantages, i.e. it allows for a detailed examination of edge-cases. Already, the scenario of hot ambient air has been described. When the ambient air is additionally dry, latent cooling may, in fact, account for more than 100% of the total cooling. Such an unusual scenario arises when the temperature of the inflowing air is larger than that of the outflowing water. Thus, paradoxically, the flow of sensible heat is from air to water rather than from water to air– see Figures 4.4 and 4.4E. A further advantage of the zone-centric model developed herein is that it allows one to estimate the height within the fill where the air first becomes saturated. This, in turn, assists in determining the required fill height for a particular output

temperature/humidity ratio. The fill height plays a vital role in designing a cooling tower; if the fill is too short, insufficient cooling might occur. But if it is too large, the length of the visible plume may increase and, in any event, additional costs (capital and operating) must be assumed. An additional merit of a zone-centric model is that a robust estimate may be derived for the volume of water evaporated from each zone in the cooling tower. Knowledge of this value is essential in determining the amount of make-up water to be supplied to maintain an appropriate degree of cooling within the industrial facility. To this end, the visible plume is, not surprisingly, expected to be most prominent when ambient conditions are categorized as cold and humid. An additional aspect of our analysis is to compare the performance of a hybrid cooling tower vs. a wet cooling tower. The latter category of tower performs most efficiently when the ambient conditions are cold and dry; this is because both wet and dry sections operate at their full capacity–see sub-section 4.4.3. For the environmental and operating conditions prescribed in tables 4.7 and 4.6, Figures 4.10A and 4.11A demonstrate that the dry section cools the hot water by 2.68 K, which is four times greater than the cooling reported in sub-sections 4.4.2 and 4.4.1, where hot /dry and hot/humid conditions are respectively considered. The enhanced performance of the dry section also reflects on the amount of water conserved. The hot air from the dry section dilutes the air from a super-saturated to sub-saturated state. Thus, Figure 4.11C indicates that the super-saturated air leaving the wet section would have generated a visible plume of height 60.2 m. If a visible plume is of this height is undesirable or, for reasons of safety and/or aesthetics, prohibited, an attached dry section can be used to successfully mitigate/e-liminate fog formation –see Figures 4.10C and 4.11C. For example, and referring to the previous example and the hybrid cooling tower calculations described in sub-section 4.4.4, the visible plume length can be decreased from 60.2 m to 0 m by addition of a heat exchanger consisting of four rows of extended bi-metallic finned tubes. To the above end, altering the fraction of air directed to the wet vs. dry sections of a cooling hybrid tower has proven to be an effective mechanism for reducing plume visibility as shown in Figures 4.12A and 4.13A. A control system can be implemented for directing the right volume of air to the wet and dry sections and this will provide industries with an opportunity to maximize thermal loads.

After quantifying the performance of a hybrid cooling tower for different ambient conditions ranging from hot/dry to cold/wet. In section 4.5, we proceed to evaluate the performance of a hybrid cooling tower for different geometrical and operating parameters. In section 4.5, we have shown how visible plume, range and water evaporation changes for different L/G ratios, fill types, fill height, and number of tubes per row in sub-sections 4.5.1, 4.5.2, 4.5.3, and 4.5.4, respectively. In sub-section 4.5.1 we have

shown how L/G ratio plays a crucial parameter in increasing the cooling range and to decrease the visible plume height. For example, in Figure 4.13A we observe that by decreasing the L/G from 2 to 0.25, the visible plume height plummets from 150 m to 40 m, and can be completely curtailed by increasing the percentage of air directed towards the dry section. On the other hand, we observe an increase in the cooling range by 17 K when the L/G is decreased from 2 to 0.25 see–Figure 4.13B. In sub-section 4.5.2, we have compared the performance of different film type fills, those produced by Brentwood Industries, Inc. In this parametric study we have examined different type of flute configurations such as cross-fluted, vertical fluted, and offset-vertical. Figures 4.14B, 4.15B, 4.14C, 4.15C shows that cross-fluted fill offers highest thermal performance followed by offset-vertical fill, and vertical fluted fill. Due to the enhanced thermal performance in the cross-fluted fill, we also observe increase in visible plume height–see Figures 4.14A, 4.15A. A parametric study varying the fill height in sub-section 4.5.3 shows that by reducing the fill height curtails the visible plume height–see Figure 4.17A, 4.16A. On the other hand, it leads to the decrease in the thermal performance of the cooling tower as shown in Figures 4.16B, 4.17B. Finally, in sub-section 4.5.4 we have shown that by increasing the number of tubes per row in the dry section the visible plume and the water evaporation can be reduced as reported in Figures 4.18A, 4.19A, 4.18C, 4.19C.

5.2 Future Work

The work summarized above offers a number of avenues for future study, which we outline in bullet point form below.

- Fouling of the fill is one of the most important factors for reducing the in performance of a wet section. Khan and Zubair [48] demonstrated that fill fouling can result in an increase of outlet water temperature by 23.5% and 18.3% for medium and small-sized cooling towers, respectively, operating under similar conditions. Therefore, and in order to assess the longer term performance of the cooling tower, a fouling model has to be implemented for the wet section. Doing so encourages engineers to consider designs that are more accommodating to fill fouling, which should, in the long run, lead to better overall performance.

- In our study, we assume complete mixing within the plenum chamber, which might lead to some inaccuracies while evaluating the actual outlet air temperature and humidity ratio. A CFD simulation can be performed to predict the mixing efficiency in the plenum chamber. By extension, such a study could be used to

understand the degree of uniformity of the stream of hot air discharged by the cooling tower to the atmosphere.

- Cooling towers account for a significant proportion of the total cost in power stations or other process industries. An ill-performing cooling tower can lead to a decrease in the overall efficiency of the industrial plant resulting in economically-unfavorable outcomes [49]. Designing a cooling tower involves a trade-off between environmental constraints, design parameters, and cost factors. Therefore, design optimization has to be considered to maximize the thermal performance and to minimize the capital and operating cost of a hybrid cooling tower. Previous analyses have explored the optimization problem in question with the objective of reducing the capital and operating costs associated with mechanical draft cooling towers. The design parameters in these optimization studies included the fill type, fill height, the mass flow rate of air, rain zone height and spray zone height [50–55]. A similar optimization framework can be extended to a hybrid cooling tower for designing wet-dry cooling towers meant to minimize fog formation in the atmosphere and avoid an excess evaporation of water within the tower itself. One can better optimize a cooling tower by introducing constraints on the design parameters. For example, (i) constraint on maximum flow rate of water; to avoid flooding of fill, (ii) minimum height of the tower; to avoid recirculation of air, and (iii) maximum allowable height of the visible plume can also be provided as a constraints.

- Blackburn et al. [56] performed a real-time optimization of an induced draft cooling tower by using a fan equipped with a variable frequency drive (VFD); by doing so, they reported a 6.7% annual energy usage savings. We have seen in sub-section 4.5.1, that the tower thermal performance and visible plume length may adjust considerably by altering the fraction of air directed to the wet vs. dry sections of a cooling hybrid tower. Thus, a study similar to, but more involved than, that of Blackburn et al. [56] could be devised for a hybrid cooling tower for designing energy-efficient towers, this for the purposes of modulating not merely the overall air flow rate but, additionally, the volume of air directed to each of the wet and dry sections.

- In this thesis, we have studied the plume evolution, considering still and uniform ambient conditions. To improve model realism, an ambient wind and stratified ambient should be considered. Previous studies have concluded that the entrainment of ambient air into the plume increases with the wind speed resulting in reduced visible plume lengths [26, 57–61]. Furthermore, plumes in a stratified environment lose buoyancy and begin to spread horizontally, when the plume

temperature is equal to the ambient temperature; a vertical level referred to as the inversion height. Hence, considering wind speed and stratified ambient in the plume model would enable a more robust prediction of a visible plume height, by extension, better cooling tower design.

Bibliography

Chapter 6

Bibliography

[1] FHY Wu and RCY Koh. Mathematical model for multiple cooling tower plumes. final report. Technical report, California Inst. of Tech., Pasadena (USA). WK Kellogg Radiation Lab., 1978.

[2] Pieter Cornelis Oosthuizen. *Performance characteristics of hybrid cooling towers*. PhD thesis, Stellenbosch: Stellenbosch University, 1995.

[3] Kristen Averyt. *Freshwater use by US power plants: Electricity's thirst for a precious resource*. Union of Concerned Scientists., 2011.

[4] D. G. Kröger. *Air-Cooled Heat Exchangers and Cooling Towers-Thermal-Flow Performance Evaluation and Design*, volume 1. PennWell, 2004.

[5] R York, M Foster, N Davis, J Schoonmaker, R Unsworth, and C Holmes. Issues and environmental impacts associated with once-through cooling at california's coastal power plants. *California Energy Commission*, 2005.

[6] Man-Him Chan. *Cooling tower performance analysis and visible air plume abatement in buildings situated in temperate climate zone*. PhD thesis, Cardiff University, 2015.

[7] Robert E Cates. Parallel air path wet-dry water cooling tower, December 2 1975. US Patent 3,923,935.

[8] J Maulbetsch. Comparison of alternate cooling technologies for us power plants: Economic, environmental, and other tradeoffs. *Electric Power Research Institute, Palo Alto, CA, USA*, 2004.

[9] Antonio Peris Alonso. Numerical simulation of a cooling tower and its plume. Master's thesis, Universitat Politècnica de Catalunya, 2019.

[10] Thomas E Croley, Mow-Soung Cheng, and VC Patel. Economic factors of dry-wet cooling towers. *Journal of the Power Division*, 102(2):147–163, 1976.

[11] WV Loscutoff. Preliminary evaluation of wet/dry cooling concepts for power plants. Technical report, Battelle Pacific Northwest Labs., Richland, Wash.(USA), 1976.

[12] Wanchai Asvapoositkul and Mantheerapol Kuansathan. Comparative evaluation of hybrid (dry/wet) cooling tower performance. *Applied Thermal Engineering*, 71 (1):83–93, 2014.

[13] Shahed Taghian Dehaghani and Hossein Ahmadikia. Retrofit of a wet cooling tower in order to reduce water and fan power consumption using a wet/dry approach. *Applied Thermal Engineering*, 125:1002–1014, 2017.

[14] F. Merkel. Verdunstungskühlung. *VDI-Zeitchrift*, 70:123–128, 1925.

[15] Jaber H and Webb RL. J. Design of cooling towers by the effectiveness-ntu method. *Heat Transfer*, 111:83, 1989.

[16] M. Poppe and H. Rogener. Berechnung von ruckkiihlwerken. VDI-Warmeatlas: Mh 1– Mh 15.

[17] A. Klimanek and R.A. Bialecki. Solution of heat and mass transfer in counterflow wet-cooling tower fills. *International Communications in Heat and Mass Transfer*, 36(6):547 – 553, 2009. ISSN 0735-1933.

[18] R. C. Jordan and G. B. Priester. *Refrigeration and air conditioning.* 1948.

[19] John Warner Sutherland. Analysis of mechanical-draught counterflow air/water cooling towers. *Journal of heat transfer*, 105(3):576–583, 1983.

[20] JL Grange. Calculating the evaporated water flow in a wet cooling tower. Technical report, Electricite de France (EDF), 1994.

[21] C Bourillot. Teferi: numerical model for calculating the performance of an evaporative cooling tower. Technical report, Electricite de France, 78-Chatou. Thermal Transfer and Aerodynamic Dept., 1983.

[22] JC Kloppers and DG Kröger. A critical investigation into the heat and mass transfer analysis of crossflow wet-cooling towers. *Numerical Heat Transfer, Part A: Applications*, 46(8):785–806, 2004.

[23] BR Morton. Buoyant plumes in a moist atmosphere. *Journal of Fluid Mechanics*, 2(2):127–144, 1957.

[24] GT Csanady. Bent-over vapor plumes. *Journal of Applied Meteorology*, 10(1): 36–42, 1971.

[25] TML Wigley and PR Slawson. On the condensation of buoyant, moist, bent-over plumes. *Journal of Applied Meteorology*, 10(2):253–259, 1971.

[26] Shuo Li, Ali Moradi, Brad Vickers, and MR Flynn. Cooling tower plume abatement using a coaxial plume structure. *International Journal of Heat and Mass Transfer*, 120:178–193, 2018.

[27] Franjo Bošnjaković. *Technical thermodynamics*. Holt, Rinehart and Winston, 1965.

[28] H.J. Lowe and D.G. Christie. Heat transfer and pressure drop data on cooling tower packings and model studies of the resistance of natural draft towers to airflow. volume Part V of *Proceedings of the International Heat Transfer Conference, Colorado*, pages 933–950, 1961.

[29] Hanno CR Reuter, Dawie J Viljoen, and Detlev G Kroger. A method to determine the performance characteristics of cooling tower spray zones. In *2010 14th International Heat Transfer Conference*, pages 619–628. American Society of Mechanical Engineers, 2010.

[30] B.M. Johnson. Cooling tower performance prediction and improvement. *Volume 1, Applications Guide, EPRI Report GS-6370, Volume 2, Base, Palo Alto*, 1989.

[31] J. C. Kloppers. A critical evaluation and refinement of the performance prediction of wet-cooling towers. *University of Stellenbosch*, Ph.D. thesis, 2003.

[32] E De Villiers and DG Kroger. Analysis of heat, mass, and momentum transfer in the rain zone of counterflow cooling towers. *Journal of engineering for gas turbines and power*, 121(4):751–755, 1999.

[33] W.E. Ranz and W.R. Marsgall. Evaporation from drops. *Chemical engineering process*, 48:141–146, 1952.

[34] Kunio Miura, Takatoshi Miura, and Shigemori Ohtani. Heat and mass transfer to and from droplets. *AIChE Symposium Series*, 73:95–102, 01 1975.

[35] J.C. Kloppers and D.G. Kröger. A critical investigation into the heat and mass transfer analysis of counterflow wet-cooling towers. *International Journal of Heat and Mass Transfer*, 48(3):765 – 777, 2005. ISSN 0017-9310. doi: https://doi.org/10.1016/j.ijheatmasstransfer.2004.09.004. URL `http://www.sciencedirect.com/science/article/pii/S0017931004004041`.

[36] Jacek Kierzenka and Lawrence F. Shampine. A BVP solver based on residual control and the Maltab PSE. *ACM Trans. Math. Softw.*, 27(3):299–316, September 2001. ISSN 0098-3500.

[37] A Ganguli, SS Tung, and J Taborek. Parametric study of air-cooled heat exchanger finned tube geometry. In *AIChE symposium series*, volume 81, pages 122–128, 1985.

[38] TE Schmidt. La production calorifique des surfaces munies d'ailettes. *Annexe Du bulletin De L'Institut International Du Froid, Annexe G-5*, 1945.

[39] JP Holman. Heat transfer (SI metric edition) mcgraw-hill. *New York*, 1989.

[40] BR Morton, Geoffrey Ingram Taylor, and John Stewart Turner. Turbulent gravitational convection from maintained and instantaneous sources. *Proceedings of the Royal Society of London. Series A. Mathematical and Physical Sciences*, 234 (1196):1–23, 1956.

[41] Christophe Bailly and Geneviève Comte-Bellot. Introduction to turbulence. In *Turbulence*, pages 1–31. Springer, 2015.

[42] PF Linden. Convection in the environment. *Perspectives in fluid dynamics: A collective introduction to current research*, pages 289–345, 2000.

[43] Judith A Curry and Peter J Webster. *Thermodynamics of atmospheres and oceans*. Elsevier, 1998.

[44] Eva Monteiro and Enrico Torlaschi. On the dynamic interpretation of the virtual temperature. *Journal of the atmospheric sciences*, 64(8):2975–2979, 2007.

[45] Robert C Koh and Loh-Nien Fan. Mathematical models for the prediction of temperature distributions resulting from the discharge of heated water into large bodies of water. 1970.

[46] Adam Klimanek. Numerical modelling of natural draft wet-cooling towers. *Archives of Computational Methods in Engineering*, 20(1):61–109, 2013.

[47] Kuljeet Singh and Ranjan Das. An experimental and multi-objective optimization study of a forced draft cooling tower with different fills. *Energy Conversion and Management*, 111:417–430, 2016.

[48] JUR Khan and SM Zubair. A study of fouling and its effects on the performance of counter flow wet cooling towers. *Proceedings of the Institution of Mechanical Engineers, Part E: Journal of Process Mechanical Engineering*, 218(1):43–51, 2004.

[49] Nicholas J Williamson. Numerical modelling of heat and mass transfer and optimisation of a natural draft wet cooling tower. 2008.

[50] M.S Söylemez. On the optimum sizing of cooling towers. *Energy Conversion and Management*, 42(7):783 – 789, 2001. ISSN 0196-8904. doi: https://doi.org/10.1016/S0196-8904(00)00148-5. URL `http://www.sciencedirect.com/science/article/pii/S0196890400001485`.

[51] R.V. Rao and V.K. Patel. Optimization of mechanical draft counter flow wet-cooling tower using artificial bee colony algorithm. *Energy Conversion and Management*, 52(7):2611 – 2622, 2011. ISSN 0196-8904. doi: https://doi.org/10.1016/j.enconman.2011.02.010. URL `http://www.sciencedirect.com/science/article/pii/S0196890411000823`.

[52] Kuljeet Singh and Ranjan Das. Simultaneous optimization of performance parameters and energy consumption in induced draft cooling towers. *Chemical Engineering Research and Design*, 123:1–13, 2017.

[53] Kuljeet Singh and Ranjan Das. An improved constrained inverse optimization method for mechanical draft cooling towers. *Applied Thermal Engineering*, 114: 573–582, 2017.

[54] Zheng Zou, Zhiqiang Guan, and Hal Gurgenci. Optimization design of solar enhanced natural draft dry cooling tower. *Energy conversion and management*, 76: 945–955, 2013.

[55] Eusiel Rubio-Castro, Medardo Serna-González, José María Ponce-Ortega, and Miguel Angel Morales-Cabrera. Optimization of mechanical draft counter flow wet-cooling towers using a rigorous model. *Applied Thermal Engineering*, 31(16): 3615–3628, 2011.

[56] Landen D Blackburn, Jacob F Tuttle, and Kody M Powell. Real-time optimization of multi-cell industrial evaporative cooling towers using machine learning and particle swarm optimization. *Journal of Cleaner Production*, 271:122175, 2020.

[57] BEA Fisher. Predicting cooling tower plume dispersion. *Proceedings of the Institution of Mechanical Engineers, Part A: Journal of Power and Energy*, 211(4): 291–297, 1997.

[58] Dennett DJ Netterville. Plume rise, entrainment and dispersion in turbulent winds. *Atmospheric Environment. Part A. General Topics*, 24(5):1061–1081, 1990.

[59] AG Clarke and CL Shaw. The evaluation of plume visibility. *Process Safety and Environmental Protection*, 71:203–203, 1993.

[60] BJ Devenish, GG Rooney, HN Webster, and DJ Thomson. The entrainment rate for buoyant plumes in a crossflow. *Boundary-layer meteorology*, 134(3):411–439, 2010.

[61] Jeffrey C Weil. Plume rise. In *Lectures on air pollution modeling*, pages 119–166. Springer, 1988.

[62] Ashrae handbook. *HVAC Systems and equipment*, Vol -20:20.1–20.16, 2008.

Appendix A

Thermophysical properties

A.1 Thermophysical properties of dry air

The equations presented below for dry air are valid from 220 K to 380 K at standard atmospheric temperature [62]

Dynamic viscosity (μ_a)

$$\begin{aligned}\mu_a = {} & 2.287973 \times 10^{-6} + 6.259793 \times 10^{-8} T - 3.131956 \times 10^{-11} T^2 \\ & + 8.15038 \times 10^{-15} T^3\end{aligned} \tag{A.1}$$

where T is the temperature of dry air measured in K and μ_a is measured in kg/(m s)

Thermal conductivity (k_a)

$$\begin{aligned}k_a = {} & 4.937787 \times 10^{-4} + 1.018087 \times 10^{-4} T - 4.627937 \times 10^{-8} T^2 \\ & + 1.250603 \times 10^{-11} T^3\end{aligned} \tag{A.2}$$

where T is the temperature of dry air measured in K and k_a is measured in W/mK

Specific heat (c_{pa})

$$\begin{aligned}c_{pa} = {} & 1.045356 \times 10^{3} - 3.161783 \times 10^{-1} T + 7.083814 \times 10^{-4} T^2 \\ & - 2.705209 \times 10^{-7} T^3\end{aligned} \tag{A.3}$$

where T is the temperature of dry air measured in K and c_{pa} is measured in J/kgK

A.2 Thermophysical properties of saturated water vapor

The equations presented below for saturated water vapor are valid from 273.15 K to 380 K at standard atmospheric pressure [62]

Vapor Pressure (P_v)

$$P_v = 10^z \tag{A.4}$$

where

$$\begin{aligned} z =& 10.79574(1 - 273.16/T) \\ & - 5.02800 \times \log_{10}(T/273.16) \\ & + 1.50475 \times 10^{-4} \times (1 - 10^{-8.2969(T/273.16)-1}) \\ & + 0.42873 \times 10^{-3} \times (10^{4.76955(1-273.16/T)} - 1) \\ & + 2.78614 \end{aligned} \tag{A.5}$$

where T is the temperature of the saturated water vapour measured in K and P_v is measured in $\mathrm{N/m^2}$

Dynamic viscosity (μ_v)

$$\begin{aligned} \mu_v = & 2.562435 \times 10^{-6} + 1.816683 \times 10^{-8}T - 2.579066 \times 10^{-11}T^2 \\ & - 1.067299 \times 10^{-15}T^3 \end{aligned} \tag{A.6}$$

where T is the temperature of the saturated water vapour measured in K and μ_v is measured in $\mathrm{kg/(m\,s)}$

Thermal conductivity (k_v)

$$\begin{aligned} k_v = & 1.3046 \times 10^{-2} - 3.756191 \times 10^{-5}T - 2.217964 \times 10^{-7}T^2 \\ & - 1.11156 \times 10^{-10}T^3 \end{aligned} \tag{A.7}$$

where T is the temperature of the saturated water vapour measured in K and k_v is measured in W/mK

Specific heat (c_{pv})

$$c_{pv} = 1.3605 \times 10^3 + 2.31334T - 2.46784 \times 10^{-10}T^5 + 5.91332 \times 10^{-13}T^6 \tag{A.8}$$

where T is the temperature of the saturated water vapour measured in K and c_{pv} is measured in J/kgK

Vapor density (ρ_v)

$$\rho_v = -4.06232 + 0.10277044T - 9.76300 \times 10^{-4}T^2 + 4.47520 \times 10^{-6}T^3 - 1.00459 \times 10^{-8}T^4 + 8.91548 \times 10^{-12}T^5 \tag{A.9}$$

where T is the temperature of the saturated water vapour measured in K and ρ_v is measured in kg/m^3

A.3 Thermophysical properties of air and water vapor

The equations presented below for air and water vapor are valid from 273.15 K to 380 K at standard atmospheric temperature [62]

Humidity ratio (ω)

$$\omega = \frac{(2501 - 2.381T_{wb})\omega_{sat} - (T - T_{wb})}{2501 + 1.805T - 4.186T_{wb}} \tag{A.10}$$

where

$$\omega_{sat} = \frac{0.6250P_{v,wb}}{(P_{abs} - 1.005P_{a,wb})}$$

Also, T is the dry bulb temperature and T_{wb} is the wet bulb temperature, both measured in Kelvin. Finally, P_{abs} is the absolute pressure and $P_{v,wb}$ is the vapor pressure measured at the wet bulb temperature.

Dynamic viscosity (μ_{av})

$$\mu_{av} = \frac{X_a\mu_a M_a^{1/2} + X_v\mu_v M_v^{1/2}}{X_a M_a^{1/2} + X_v M_v^{1/2}} \tag{A.11}$$

where $M_a = 28.97$ kg/mol, $M_v = 18.016$ kg/mol,

$$X_a = 1/(1 + 1.608\omega) \qquad \text{and} \qquad X_v = \omega/(1.608 + \omega)$$

where μ_{av} is measured in kg/(m s)

Thermal conductivity (k_{av})

$$k_{av} = \frac{X_a k_a M_a^{1/3} + X_v k_v M_v^{1/3}}{X_a M_a^{1/3} + X_v M_v^{1/3}} \tag{A.12}$$

where T is the temperature of the saturated water vapour measured in K and k_{av} is measured in W/mK

Specific heat (c_{pav})

$$c_{pav} = \frac{(c_{pa} + \omega c_{pv})}{1 + \omega} \tag{A.13}$$

where T is the temperature of the saturated water vapour measured in K and c_{pav} is measured in J/kgK

A.4 Thermophysical properties of water

The equations presented below for water are valid from 273.15 K to 380 K at standard atmospheric temperature [62]

Specific heat (c_w)

$$\begin{aligned} c_{pw} = {} & 8.15599 \times 10^3 - 2.80627 \times 10T + 5.11283 \times 10^{-2} T^2 \\ & - 2.17582 \times 10^{-13} T^6 \end{aligned} \tag{A.14}$$

where T is the temperature of the water measured in K and c_{pw} is measured in J/kgK

Density (ρ_w)

$$\begin{aligned} \rho_w = {} & (1.49343 \times 10^{-3} - 3.7164 \times 10^{-6} T + 7.09782 \times 10^{-9} T^2 \\ & - 1.90321 \times 10^{-20} T^6)^{-1} \end{aligned} \tag{A.15}$$

where T is the temperature of the water measured in K and ρ_w is measured in kg/m^3

Latent Heat of Evaporation (r)

$$\begin{aligned} r = {} & 3.4831814 \times 10^{6} - 5.8627703 \times 10^{3} T + 12.139568 T^{2} \\ & - 1.40290431 \times 10^{-2} T^{3} \end{aligned} \tag{A.16}$$

where T is the temperature of the water measured in K and r is measured in J/K

Surface Tension (σ_w)

$$\begin{aligned} \sigma_w = {} & 5.148103 \times 10^{-2} + 3.998714 \times 10^{-4} T - 1.4721869 \times 10^{-6} T^{2} \\ & + 1.21405335 \times 10^{-9} T^{3} \end{aligned} \tag{A.17}$$

where T is the temperature of the water measured in K and σ_w is measured in N/m

Appendix B

CoolIT

B.1 Introduction

An open-source numerical tool, CoolIT, is developed to evaluate the performance of wet and hybrid cooling towers and to assess the severity of their plumes. To this end, we have implemented the Merkel and augmented models into CoolIT for analyzing wet cooling towers operating in a counterflow configuration. Furthermore, the e-NTU model is implemented to predict the heat transfer processes that occur within an air-cooled heat exchanger (hybrid cooling tower). Finally, to forecast the likelihood of visible formation and to predict the height of visible plume, an integral turbulent plume model is adapted from the work of Wu and Koh [1]. CoolIT was developed in collaboration with our industrial partner International Cooling Towers, Inc. Table B.1 describes the contribution of researchers in developing CoolIT.

Table B.1: CoolIT contributors

Contributors	Contribution
James Cook, Lisa Clare, and Prashanth Karupothula	Implemented the Merkel model, GUI, and implemented the thermophysical properties
Shuo Li, Harshil Pisavadia, and Antonio Peris	Implemented single and multiple plume models and integrated these with the cooling tower models
Aditya Kodkani	Implemented the augmented model and the e-NTU model

B.2 Numerical implementation

CoolIT is a python based package, written using object-oriented programming, that contains a number of classes that interact with one another. The augmented model has been divided into the following classes: *Klimanek-equation.py*, *Klimanek.py*, and *Klimanek-post-processing.py*. The former is a collection of all the equations required for predicting the thermodynamic properties of a wet cooling tower, i.e. (2.6), (2.7), (2.14) and (2.15) for unsaturated air and (2.18-2.24) for supersaturated air. In *Klimanek.py*, we solve the governing equations by evaluating zone specific Merkel numbers for the rain, fill, and spray zones. The equations are integrated along the cooling tower height, depending on the condition either equations for saturated air, (2.6 -2.7), (2.14 - 2.15) or supersaturate air (2.21-2.24) are invoked. A Python based BVP solver, "solve_bvp". Thereby we recover key thermodynamic properties such as the mass flow rate of water, temperature of water, temperature of air, and humidity ratio. Finally, the proportion of latent and sensible heats rejected in different cooling tower zones are evaluated using *Klimanek-post-processing.py*.

For a hybrid cooling tower, the e-NTU model and wet cooling tower model, either Merkel or augmented model, are solved in a sequential order. The e-NTU model has been divided into the following classes: *DryCooling.py*, *Dry-cooling-equations.py* and *Effectiveness-equations.py*. *Dry-cooling-equations.py* calculates the air and waterside heat transfer coefficients. The calculated heat transfer coefficients are provided as inputs to *Dry-cooling.py* for evaluating the outlet water and air temperatures. Finally, *Effectiveness-equations.py* contains equations to calculate the effectiveness of the heat exchanger for different flow configurations such as counterflow, parallel flow, and cross-flow unmixed.

The multiple plume code is divided into three classes: *plume-solver-multiple.py*, *line-plume.py*, and *round-plume.py*. After solving the cooling tower model, the input parameters required to solve the plume model are provided as an input to *plume-solver-multiple.py*. The *plume-solver-multiple.py* class evaluates the different permutations that may be associated with the evolution of the plume. These include onset of condensation prior to plume merger, onset and termination of condensation prior to plume merger and delayed (or no) condensation by which merger occurs before the appearance of any liquid water droplets. Equations (3.37 -3.40) are integrated in z up to some prescribed elevation using Python's "odelay" function. During the process of integration, the classes defined by *line-plume.py* and *round-plume.py* are invoked depending upon

whether the plume has or has not yet merged with those plumes emitted by adjacent cooling tower cells.